A MEASUREMENT OF B^0–$\overline{B}^0$ MIXING IN $e^+ e^-$ ANNIHILATION AT 29 GeV

Thesis by

Andrew J. Weir

In Partial Fulfillment of the Requirements
for the Degree of
Doctor of Philosophy

California Institute of Technology
Pasadena, California

1990

(Submitted October 31st, 1989)

It is a pleasure to acknowledge the people who have helped make this thesis possible.

At Caltech, I would like to thank my advisor, Barry Barish, for his support and guidance, and the members of the Caltech Mark II group, especially Frank Porter, Eric "Wild Man" Soderstrom and Ryszard Stroynowski.

At SLAC, I would like to thank the members of the Mark II collaboration, notably Jonathan Dorfan, Art Snyder and Steve Wagner.

At Oxford, I would like to thank Roger Cashmore.

I would particularly like to thank Chris Hawkes, Mark Nelson and René Ong for all their advice and help, without whom, *etc.*, *etc.*

Most of all, I would like to thank my wife, Helen, and my parents for their unequivocal love and support.

This thesis was produced on a Macintosh™ computer using FullWrite Professional,™ Expressionist™ and Canvas™ and is typeset in Goudy Old Style. TEX

This thesis describes a measurement of $B^0-\overline{B}^0$ mixing in events produced by electron-positron annihilation at a center of mass energy of 29 GeV. The data were taken by the Mark II detector in the PEP storage ring at the Stanford Linear Accelerator Center between 1981 and 1987, and correspond to a total integrated luminosity of $224 pb^{-1}$.

We used a new method, based on the kinematics of hadronic events containing two leptons, to provide a measurement of the probability, χ, that a hadron, initially containing a b ($\overline{b}$) quark decays to a positive (negative) lepton to be $\chi = 0.17^{+0.15}_{-0.08}$, with 90% confidence level upper and lower limits of 0.38 and 0.06, respectively, including all estimated systematic errors. Because of the good separation of signal and background, this result is relatively insensitive to various systematic effects which have complicated previous measurements.

We interpret this result as evidence for the mixing of neutral B mesons. Based on existing B^0_d mixing rate measurements, and some assumptions about the fractions of B^0_d and B^0_s mesons present in the data, this result favors maximal mixing of B^0_s mesons, although it cannot rule out zero B^0_s mixing at the 90% confidence level.

Chapter 1

Introduction

THIS thesis presents a measurement of "B-mixing" — the phenomenon whereby a neutral meson containing a bottom quark can spontaneously change into its antiparticle. The measurement relies on the ability to identify events in which two hadrons containing bottom quarks decay semileptonically to electrons or muons, and the theoretical expectation that the charges of these leptons are correlated with the charges of their bottom-quark parents. If there were no B-mixing, the two leptons from the bottom-quark decays would always have opposite signs; if there is a lot of mixing, the charges of the two leptons will be uncorrelated with each other.

Quarks, hadrons, leptons, etc.

One of the greatest achievements of 20th century physics has been the development of a theoretical framework within which almost all observable phenomena can be accommodated. The most elementary constituents of matter and their interactions are specified by the *Standard Model*[1]. This model prescribes four fundamental forces and three families of particles. The lightest, and most stable family constitutes the long-lived material which we observe in the universe, namely protons, neutrons, electrons and (electron) neutrinos. The protons and neutrons are composed of the more elementary *up* and *down* quarks, while the electron and electron neutrino are believed to be elementary. The less stable, heavier quarks and leptons are generally only observed in cosmic rays and their interaction with the atmosphere, and in particle-beam experiments.

The Standard Model provides for the union of the *electromagnetic* and *weak* interactions into the *electroweak* theory. The interactions specified by this theory, along with the *strong* interaction specified by Quantum Chromodynamics (QCD), govern all the phenomena associated with the production and decay of B hadrons.

The quarks and leptons form three generations of spin 1/2 fermions. The leptons do not experience the strong interaction, while the quarks interact primarily through the strong force, which binds them into mesons (a quark anti-quark pair), and baryons (three quarks or antiquarks)†. The three generations are shown in Table 1. 1. The top quark and the tau neutrino have not been experimentally observed. For each particle shown there is a corresponding anti-particle with the opposite electric charge.

	electric charge	*generation I*	*generation II*	*generation III*
quarks	+ 2/3	up (*u*)	charm (*c*)	top (*t*)
	– 1/3	down (*d*)	strange (*s*)	bottom (*b*)
leptons	0	neutrino (ν_e)	neutrino (ν_μ)	neutrino (ν_τ)
	– 1	electron (*e*)	muon (μ)	tau (τ)

Table 1. 1

The particles can change generations through the *weak* interaction by exchanging the *gauge quanta* of the weak interaction, namely the charged $W^{\pm}$ (the other weak gauge quantum, the Z^0, mediates neutral current processes). Because of the relative weakness of the gravitational interaction, it plays essentially no part in this experiment.

† Mesons and baryons are collectively referred to as *hadrons*.

Production of B hadrons

Pairs of quarks are produced by e^+e^- annihilation at energies above a few GeV. The Feynman diagram governing the dominant, one-photon exchange process is shown in Figure 1. 1†.

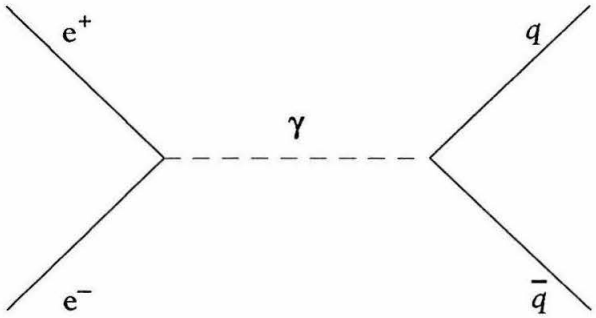

Figure 1. 1

The cross section for $q\bar{q}$ production via one-photon exchange (neglecting finite mass effects) is given by :

$$\sigma(e^+e^- \rightarrow q\,\bar{q}) = 4\pi \frac{\alpha^2 Q^2}{E_{cm}^2}$$

where : $\alpha \approx 1/137$, the *fine structure constant*,
Q is the quark charge,
E_{cm} is the center of mass energy of the e^+e^- annihilation.

From this expression, we can see that the cross section depends on the square of the quark charge, and therefore bottom quarks form 1/11 of the total $q\bar{q}$ sample. The produced "bare" quarks quickly "dress" themselves into hadrons through a process called *fragmentation*. The current understanding of this fragmentation process is mainly phenomenological due to an inability to calculate accurately the non-perturbative aspects of QCD. One model of fragmentation is that $Q\overline{Q}$ pairs are produced from the vacuum as shown in Figure 1. 2. The "string" connecting the $Q\overline{Q}$ pair represents the color field lines. As the string increases in length, the stored energy in the color field becomes large enough to create a $q\bar{q}$ pair (representing any kinematically allowed quark flavor) from

† At energies greater than about 70 GeV the Z^0 exchange term becomes important.

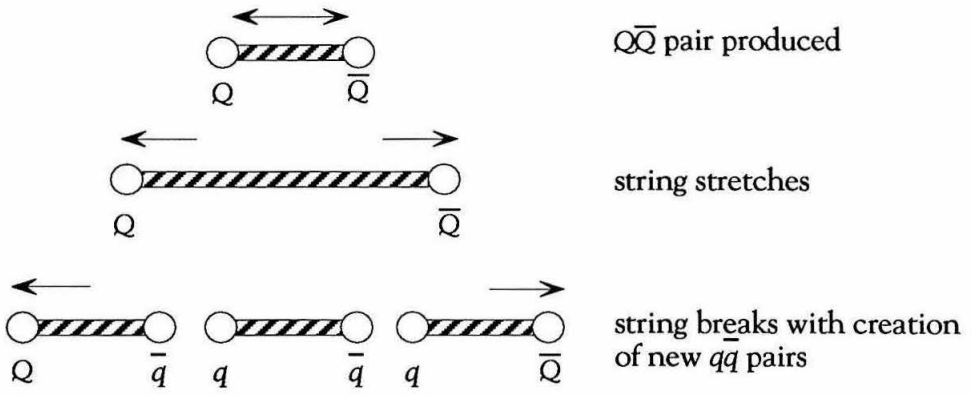

Figure 1. 2

the vacuum. This breaks the string, and the process repeats until there is not enough energy left to form $q\bar{q}$ pairs.

The *fragmentation function* is a phenomenological parametrization of the extent to which the produced hadron carries the parent quark's energy and momentum. A popular such function is the Peterson[2] parametrization :

$$f(z) \equiv \frac{1}{z\left(1 - \frac{1}{z} - \frac{\varepsilon}{(1-z)}\right)^2}$$

$$z \equiv \frac{(E + p_l)_{hadron}}{(E + p_l)_{quark}}$$

where E is the hadron energy and p_l is the momentum along the quark direction. The parameter, ε, depends on the quark flavor. Because of the heavy b quark mass (about 5 GeV/c^2), one expects B hadrons to carry off a larger fraction of the b quark energy than would hadrons from the fragmentation of lighter quarks. This has been observed experimentally in the momentum spectra of leptons produced from semileptonic C and B hadron decays[3], and by the reconstruction of the decays of D^* mesons[4]. The Monte Carlo lepton momentum spectra from semileptonic decays of C and B hadrons are strongly affected by the values of the ε parameter chosen for the c and b quark fragmentation func-

tions. From a previous Mark II inclusive lepton analysis[3] the value of ε for *b* quark fragmentation was determined to be 0.005. From exclusive charm measurements, and inclusive lepton analyses from e^+e^- annihilation at 29 GeV and above, the charm ε parameter has a value of approximately 0.05.

B hadron decay

In this thesis we consider only the *semileptonic* decays of B hadrons. The simplest Feynman diagram for such decays is the *spectator* diagram shown in Figure 1. 3.

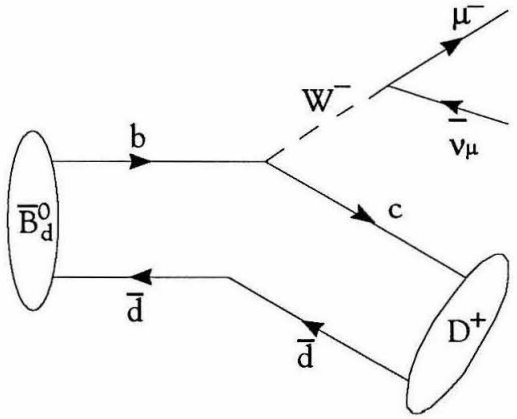

Figure 1. 3

In Figure 1. 3 the $\bar{d}$ quark acts as a spectator in that it plays no role in the decay. The charge of the lepton produced by the decay of the W is correlated with that of the parent *b* quark — the *b* quark decays produce a negative lepton, while the $\bar{b}$ quark decays produce a positive lepton. This is the basis of the method used in this thesis to distinguish between the decays of hadrons containing *b* and $\bar{b}$ quarks. In this thesis we refer to the lepton from the semileptonic decay of a *b* or $\bar{b}$ quark decay as a "B-primary" lepton. Semileptonic decays of charm quarks in $b\bar{b}$ events are referred to as "B-secondary" decays. The fact that B hadrons are not stable and decay to other quark families provides evidence that that the weak eigenstates are not the quark mass eigenstates. The Kobayashi-Maskawa (K-M) matrix[5] connects the quarks with the weak eigenstates, and is the generalization of the GIM[6] scheme to the three quark families of the Standard Model.

$$\begin{pmatrix} d' \\ s' \\ b' \end{pmatrix} = \begin{pmatrix} V_{ud} & V_{us} & V_{ub} \\ V_{cd} & V_{cs} & V_{cb} \\ V_{td} & V_{ts} & V_{tb} \end{pmatrix} \begin{pmatrix} d \\ s \\ b \end{pmatrix}$$

Where the primed quarks have been "rotated" by the 3x3 K-M matrix, and enter the weak current associated with the W^- which mediates *b* quark decays :

$$J_-^\mu = C(\,\bar{u}\;\;\bar{c}\;\;\bar{t}\,)\gamma^\mu(1-\gamma_5)\begin{pmatrix} d' \\ s' \\ b' \end{pmatrix}$$

$$+\; C(\,\bar{\nu}_e\;\bar{\nu}_\mu\;\bar{\nu}_\tau)\gamma^\mu(1-\gamma_5)\begin{pmatrix} e^- \\ \mu^- \\ \tau^- \end{pmatrix}$$

Where $C = \sqrt[3]{2}\;\sqrt{G_F}\,m_W$

The exact calculation of the B hadron decay rate is more complicated than suggested by Figure 1. 3 alone. There are various QCD corrections and finite mass effects which alter the result (although the magnitude of these corrections is expected to be significantly smaller than for the semileptonic decay of C hadrons in which the D^+ and D^0 lifetimes differ by about a factor of two[7]). Current experimental measurements suggest that the difference between the charged and neutral B hadron lifetimes is not more than a factor of two[7,8].

The mean lifetime of the B hadrons produced in e^+e^- annihilation at energies well above the Upsilon resonances has been measured to be $1.31\,^{+0.14}_{-0.13}$ picoseconds[7]. The exact composition of this ensemble of B hadrons has not been determined, which complicates the measurement of mixing in the B^0_d and B^0_s systems. The current expectation is that about 40% of the hadrons are $B^\pm$, about 40% are B^0 and $\overline{B}^0$, and the remainder are B baryons. The relative proportions of B^0_d and B^0_s are expected to be about 3:1.

Mixing phenomenology

The mixing of neutral mesons is a purely quantum mechanical phenomenon. In general, if we have a neutral meson, X^0, and its antiparticle, $\overline{X}^0$ (distinct from X^0), we can define linear combinations of these mesons which are the eigenstates of the weak Hamiltonian, $\mathbf{H}_{weak}$:

$$\mathbf{H}_{weak} = \mathbf{M} + i\,\Gamma$$

$$\lambda_\alpha = m_\alpha + i\frac{\Gamma_\alpha}{2} \; ; \; \alpha = 1, 2$$

Where $\mathbf{M}$ and Γ are the hermitian mass and decay matrices, and the eigenstates, X_1 and X_2, have eigenvalues λ_1 and λ_2, respectively. The quantities m_α and Γ_α are the mass and decay width of the weak eigenstates. The time evolution of the state X_α is then given by:

$$\begin{aligned} |X_\alpha(t)\rangle &= |X_\alpha(0)\rangle \cdot exp\left(i\,\lambda_\alpha\, t\right) \\ &= |X_\alpha(0)\rangle \cdot exp\left(-\frac{\Gamma_\alpha}{2}t\right) \cdot exp\left(i\,m_\alpha\, t\right) \end{aligned}$$

Since we are assuming that CP and T are symmetries of $\mathbf{H}_{weak}$, the quark states X^0 and $\overline{X}^0$ are related to the states X_1 and X_2 in the following manner:

$$|X^0\rangle = \frac{1}{\sqrt{2}}\left(|X_1\rangle + |X_2\rangle\right)$$

$$|\overline{X}^0\rangle = \frac{1}{\sqrt{2}}\left(|X_1\rangle - |X_2\rangle\right)$$

The time evolution of the amplitude, $\psi_0(t)$, of the X^0 state is then given by:

$$\begin{aligned} \psi_0(t) &= \frac{1}{\sqrt{2}}\left(\psi_1(t) + \psi_2(t)\right) \\ &= \frac{1}{\sqrt{2}}\left[\, exp\left(-\frac{\Gamma_1}{2} + i\,m_1\right)t + exp\left(-\frac{\Gamma_2}{2} + i\,m_2\right)t\right] \end{aligned}$$

The time evolution of the intensity for an initially pure X^0 state is given by :

$$\begin{aligned}\psi_0(t)\cdot\left(\psi_0(t)\right)^* &= \tfrac{1}{2}\left(\psi_1(t)+\psi_2(t)\right)\cdot\left(\psi_1(t)+\psi_2(t)\right)^* \\ &= \tfrac{1}{2}\Big[\, exp\left(-\Gamma_1 t\right) + exp\left(-\Gamma_2 t\right) + \\ &\qquad \underbrace{2\,exp\left(-\tfrac{1}{2}\left(\Gamma_1+\Gamma_2\right)t\right)\cdot cos\left(m_1-m_2\right)t}_{\text{interference term}}\Big]\end{aligned}$$

The interference term is the unambiguous evidence for mixing. In order to observe the effect of this interference term (assuming one can experimentally distinguish between X_1 and X_2) the difference in mass of the two states, $\Delta m = m_1 - m_2$, must be at least comparable in magnitude to the mean decay rate, $\frac{1}{2}\left(\Gamma_1+\Gamma_2\right)$. Also, in order to be experimentally accessible, the decay rate should be small enough that the mesons can travel at least a few tens of microns in the lab frame before decaying. (The neutral kaon system is particularly interesting[9] since the decay rates for the weak eigenstates are very different. This has led to several beautiful experiments on the K^0–$\overline{K}^0$ system, including the discovery of CP violation[9,10].)

In the absence of top quarks there are four neutral combinations of two quarks which can mix with their antiparticles, namely $s\bar{d}$, $c\bar{u}$, $b\bar{d}$ and $b\bar{s}$. These are the $\overline{K}^0$, D^0, $\overline{B}^0_d$ and $\overline{B}^0_s$ mesons, respectively. In order to estimate the degree of mixing these mesons are expected to undergo, we examine the process by which the mass difference, Δm, between the weak eigenstates is generated.

Since the transformation between meson and antimeson involves a $\Delta S = 2$, $\Delta C = 2$ or $\Delta B = 2$ transition, these processes are second order weak transitions. The "box diagrams" which describe the transition of a neutral meson, X^0, containing quarks q_α and $\bar{q}_\beta$ into its antimeson, $\overline{X}^0$, are shown in Figure 1. 4.

In order to conserve charge at the $W^\pm$ vertices, the intermediate quarks, q_γ and q_δ, are "up" type if q_α and $\bar{q}_\beta$ are "down" type, and *vice versa.*

Diagrams for neutral meson mixing

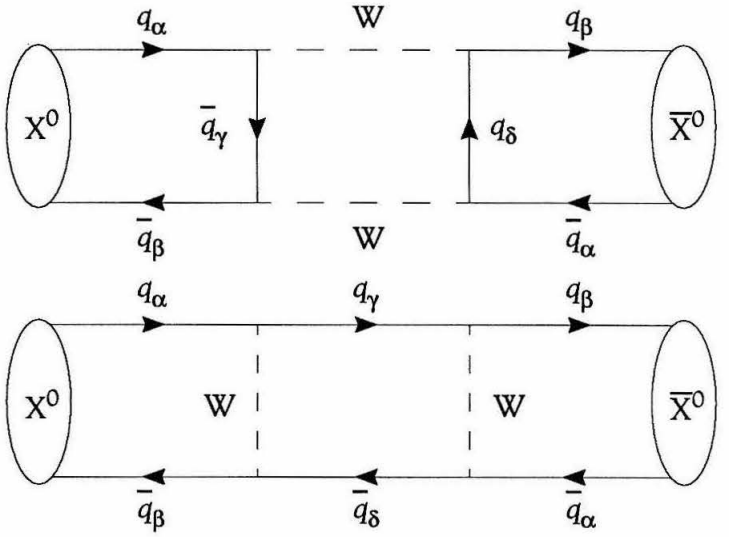

$$\Delta m \sim \sum_{\text{all possible } \gamma,\, \delta} m_{q_\gamma} \left| V_{\alpha\gamma} V_{\gamma\beta} \right| \cdot m_{q_\delta} \left| V_{\alpha\delta} V_{\delta\beta} \right|$$

Figure 1. 4

To incorporate the effect of the weak mixing angles at the W boson vertices, we use a simplified version of the Wolfenstein[11] parametrization of the K-M matrix :

$$\begin{pmatrix} V_{ud} & V_{us} & V_{ub} \\ V_{cd} & V_{cs} & V_{cb} \\ V_{td} & V_{ts} & V_{tb} \end{pmatrix} \approx \begin{pmatrix} 1 & \lambda & \lambda^3 \\ -\lambda & 1 & \lambda^2 \\ -\lambda^3 & -\lambda^2 & 1 \end{pmatrix}$$

where $\lambda \approx \sin\theta_c \approx 0.23$

The dominant terms for Δm for the four neutral meson systems are shown in Table 1. 2. Because B_d^0 mixing involves weak transitions across two generations, while B_s^0 mixing involves transitions across only one generation, we expect substantially more B_s^0 than B_d^0 mixing. Also, given that the D^0 lifetime is almost 100 times smaller than the K_s^0 life-

system	*mass difference*	$1 / \Gamma_1$ (s)	$1 / \Gamma_2$ (s)	$\Delta m / \Gamma$
K^0–$\overline{K}^0$	$\sim \lambda^2 (m_c^2 + m_s^2)\, m_K$	$9 \cdot 10^{-11}$	$5 \cdot 10^{-8}$	0.5, 277
D^0–$\overline{D}^0$	$\sim \lambda^2\, m_s^2\, m_D$	$4 \cdot 10^{-13}$	$4 \cdot 10^{-13}$	< 0.005
B^0_d–$\overline{B}^0_d$	$\sim \lambda^6\, m_t^2\, m_B$	$13 \cdot 10^{-13}$	$13 \cdot 10^{-13}$	~ 0.7
B^0_s–$\overline{B}^0_s$	$\sim \lambda^4\, m_t^2\, m_B$	$13 \cdot 10^{-13}$	$13 \cdot 10^{-13}$	~ 3

Table 1. 2

time, it is expected that the extent of mixing in the D^0 system would be relatively small. In Table 1. 2 we show the experimentally determined values of $\Delta m / \Gamma$ for the K^0, D^0 and B^0_d systems.

Because of the strong dependence of Δm on the mass of the virtual quarks, these diagrams were originally used to predict the charm quark mass[12]. Substantial mixing has been measured in the B^0_d system by the ARGUS[13] and CLEO[14] collaborations, but current theoretical uncertainties lead to somewhat imprecise predictions for the top quark mass[15]. Mixing systems are also a promising place to look for extensions beyond the Standard Model such as non-minimal Higgs models in which, for example, the W bosons in Figure 1. 4 could be replaced by charged Higgs bosons.

B-mixing

Due to the very short B hadron lifetime, and the problems of reconstructing B decays, it has not yet been possible to observe the oscillation of the "bottomness" of the hadrons. We can therefore only observe the time-integrated rate of mixing. This rate is given by the following expressions, where we have assumed that the two mass eigenstates have the same decay widths, Γ, and we ignore CP violating effects.

$$I(B^0) = \frac{e^{-\Gamma t}}{2}[1 + \cos(\Delta m t)]$$

$$I(\overline{B}^0) = \frac{e^{-\Gamma t}}{2}[1 - \cos(\Delta m t)]$$

$$\chi(B^0) = \frac{\int_0^\infty I(\overline{B}^0)\,dt}{\int_0^\infty [I(B^0) + I(\overline{B}^0)]\,dt} = \frac{\left(\frac{\Delta m}{\Gamma}\right)^2}{2 + 2\left(\frac{\Delta m}{\Gamma}\right)^2}$$

Where $I(B^0)$ is the fraction of B^0 mesons remaining at time t from a pure B^0 source at time t=0, Γ is the B decay rate, and χ is the time integrated fraction of B^0 which have mixed. Clearly, there is competition between the rate at which the B^0–$\overline{B}^0$ decay, and the rate at which they mix. If the decay rate is large, the observable mixing effects will be small.

We define the experimentally observable quantity, χ, which is the fraction of <u>all</u> semileptonic B decays (not just the neutral mesons) which produce a lepton of the "wrong" sign. Because of the correlation between the lepton sign and the parent b quark charge, this definition for χ is analogous to the one above.

$$\chi \equiv \frac{\Gamma(B \to l^- X)}{\Gamma(B \to l^\pm X)}$$

Where, using the standard convention[7], a B hadron contains a $\overline{b}$ quark, and a $\overline{B}$ hadron contains a b quark, and gamma represents the time-integrated rate. Given a pure sample of events in which both bottom quarks decay directly to leptons (B-primary decays), the fraction of like-sign events is given by $2\chi(1-\chi)$, where we assume that the B hadrons produced by fragmentation are uncorrelated, and that they undergo mixing without interference.

This measurement

Previous analyses of e^+e^- annihilation data above the Upsilon resonances have relied on the estimation of the original quark directions to separate leptons from B decay from all others. Because of the relatively large *b* quark mass, the leptons from semileptonic B decays tend to have larger momenta and to make larger angles with the original quark direction than, for example, leptons from C hadron decays. This estimation of the original quark direction relied on reconstructing the event "thrust axis," the direction in space, **n**, which maximized the quantity :

$$T = max\left[\frac{\sum_i |\mathbf{p}_i \cdot \mathbf{n}|}{\sum_i |\mathbf{p}_i|}\right]$$

where the summation is over all the charged tracks in the event, and $\mathbf{p}_i$ are the track momenta. The thrust axis was then taken as the best estimate of the original quark directions. Clearly there are problems with this estimate — in events with hard gluon radiation, the event will not have a two-jet topology. Also, missing energy in the form of neutrinos and other neutral particles will make the direction estimate imprecise. Apart from such problems with the thrust axis approach, the previous Mark II B-mixing analysis was a generalization of results from the single lepton analysis, and did not specifically address the kinematics of the dileptons themselves.

In this thesis we take a different approach, and attempt to use the kinematic correlations that exist between the two leptons. Our method does not rely on being able to estimate the original quark directions, and hence the method is also applicable to events with more than two jets.

Isolation, clusters and transverse momentum

Previous B-mixing analyses have relied on a variable known as *transverse momentum*, or p_t, to statistically separate the leptons from the decays of B and C hadrons. This variable was defined as the component of a track's momentum perpendicular to the thrust axis. In principle, if the thrust axis was a perfect estimator of the quark's initial direction and

fragmentation effects were ignored, the mean value of the transverse momentum distribution should have been proportional to the parent quark mass. In practice, the distribution is fairly broad, and, in a previous analysis[16], a simple cut of $p_t > 1\text{GeV/c}$ for leptons with $p > 2\text{GeV/c}$ gave a sample of leptons (in e^+e^- events at 29 GeV containing one lepton) of about 50-60% B-primary leptons.

The previous Mark II B-mixing analysis used these single-lepton data to estimate the purity of events in which *both* leptons had high p_t. Unfortunately, this method ignored the possible p_t correlations which exist in dilepton events, since a high momentum track will tend to "pull" the thrust axis toward itself, affecting the measured p_t of the other lepton.

In this analysis we abandoned the thrust axis method in favor of a more general estimator of the parton structure of hadronic events. We used the standard Mark II routine for finding particle clusters in hadronic events[17]. The algorithm used all possible pairs i, j of charged particles in the event *excluding the candidate leptons*, combining the pair with the lowest invariant mass to form a "pseudoparticle" with four momentum $p_{ij} = (p_i + p_j)$. Further pairing of particles and pseudoparticles with the lowest invariant masses continued until the invariant mass of all remaining pseudoparticles (which may consist of many particle pairs) was above a given threshold. These remaining pseudoparticles were called clusters (or jets). The number of reconstructed clusters clearly depends on the threshold value; a larger threshold value will result in fewer clusters, a smaller value will result in more clusters. In this analysis, we used a value of the threshold given by :

$$\textit{Cluster threshold} = \left(\frac{M_{ij}}{E_{visible}}\right)^2 = 0.05$$

Where M_{ij} is the invariant mass of a pseudoparticle, and $E_{visible}$ is the total visible energy of all charged particles in the event.

In analogy with the previous definition of transverse momentum, we then calculated the component of the lepton's momentum which was perpendicular to the direction of the nearest reconstructed cluster. In events where there was no cluster within 90° of the lepton, we assigned a very large, default value for the lepton p_t (so that the minimum transverse momentum of the dilepton pair was determined by the other lepton).

> In this analysis we use the term *transverse momentum*, or p_t , to refer to the component of the momentum of a track which is perpendicular to the direction of the *nearest charged particle cluster*.

We used three specific features of the leptons from semileptonic B decays to construct two variables associated with each lepton pair which we used to statistically separate events in which both leptons come from "primary" B hadron decay (*i.e.*, decay of the bottom quark) from all others. It is these events in which we expect to see the maximum sensitivity to mixing — if the separation were complete, we could simply count the number of like- and unlike-sign lepton pairs which would give us a measure of χ directly. These features are :

- The leptons from B-primary decays tend to have high momentum.
- These leptons tend to be relatively isolated from other tracks in the event.
- In two-jet events, these leptons are relatively acollinear.

Based on our definition of transverse momentum, and on the other dilepton observables, namely the momenta of the leptons and their acollinearity, we defined the variables shown in Figure 1. 5.

It should be stressed that these variables do not depend on the estimation of the original quark directions, but rather on observables of the dileptons themselves, independent of the number of jets in the event. The first variable, *momentum cross product*, is the magnitude of the vector cross product of the lepton momenta. Because it is quadratic in the lepton momenta it has a relatively large value for events where both leptons have large momenta. The factor $sin\theta$ is small for events in which the leptons are collinear, but relatively large for the acollinear leptons from B-primary decays. The second variable, *minimum transverse momentum*, is the smaller of the two values of the component of the lepton's momentum perpendicular to the direction of the nearest charge particle cluster in the event. Hence, if both leptons have high momenta and are isolated from the other

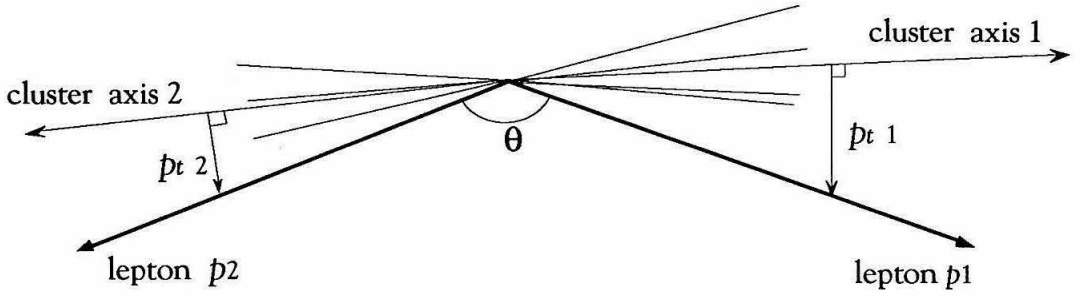

momentum cross product = $| p1 \cdot p2 \cdot \sin\theta |$

minimum transverse momentum = $min (pt1, pt2)$

Figure 1. 5

tracks in the event, this variable will be large. If *either* lepton is not isolated, or has low momentum, this variable will be small.

We would therefore expect that signal events (where both leptons are from B-primary decays) would have large values of these two variables, while background events would have small values for one, or both, of them.

Outline of thesis

The Mark II detector, and the elements used for lepton identification are described in Chapter 2. The algorithms used for lepton identification, and the estimation of lepton backgrounds are described in Chapter 3. We discuss the hadronic event selection in Chapter 4. The inclusive lepton analysis used to determine the composition of the dilepton sample is described in Chapter 5. The measurement of the mixing parameter, χ, is described in Chapter 6. Systematic effects which need to be considered in the mixing measurement are discussed in Chapter 7. Finally, Chapter 8 discusses the implications of this measurement on the current knowledge of $B^0-\overline{B}^0$ mixing.

Chapter 2

The Mark II detector

THE Mark II detector has been described in many previous publications[18]. We provide here a description of the elements necessary for the identification of multi-hadronic events, and, within these, the identification of leptons.

The Mark II detector was originally designed and built by a collaboration of scientists and engineers from the Stanford Linear Accelerator Center (SLAC) and the Lawrence Berkeley Laboratory (LBL). It has had a long and successful history at SLAC dating back to 1977 when the detector was originally installed in the SPEAR storage ring. The data used in this thesis were taken in the PEP e^+e^- storage ring between 1981 and 1987 at a center of mass energy of 29 GeV, and correspond to a total integrated luminosity of 223 pb^{-1}.

The PEP storage ring

The PEP (Positron Electron Project) e^+e^- storage ring at the Stanford Linear Accelerator Center was commissioned in 1979. Three bunches of electrons and three bunches of positrons with energies of 14.5 GeV circulated in opposite directions in the 2.2km circumference ring. There were six "interaction points" (IPs) at which, every 2.4μs, the bunches passed through each other. Typical beam cross sections at the Mark II IP were 400μm in x, 70μm in y and 1.5cm in z, while typical beam currents and luminosities were 25mA and 10^{31} cm^{-2} s^{-1}, respectively.

The Mark II detector is shown in Figure 2. 1.

The Mark II detector viewed down the beam line

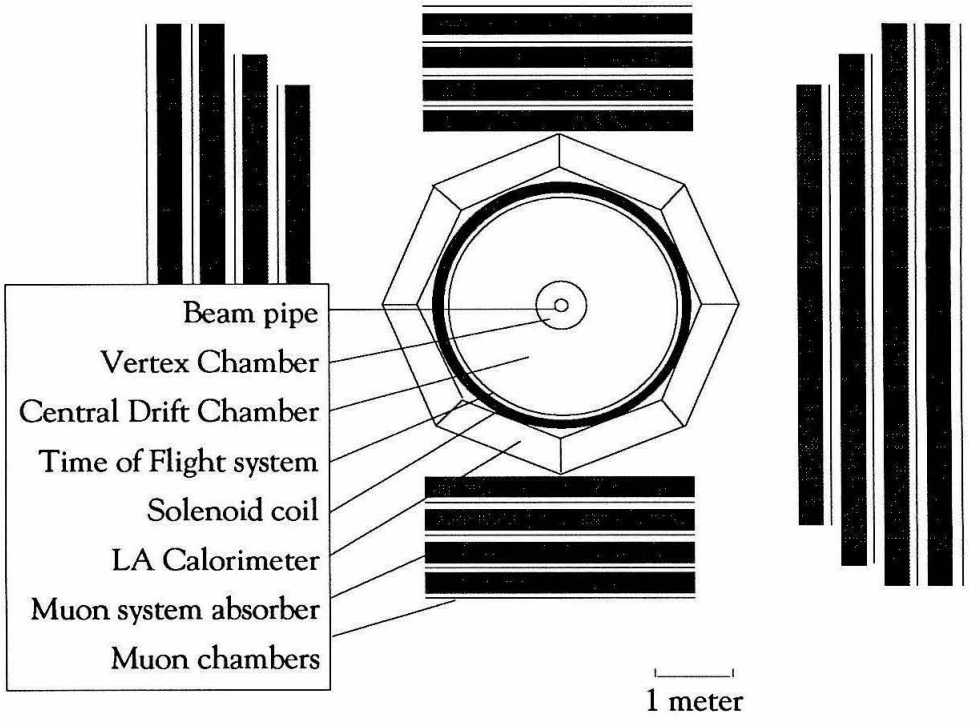

Figure 2. 1

The Drift Chambers[19]

Both Drift Chambers were used in providing precise information about the direction and curvature of the charged tracks produced at the IP. The track reconstruction software used hits in both chambers to find tracks and fit them to piecewise helical trajectories. The addition of data from the Vertex Chamber improves the momentum resolution substantially. Because this thesis relies on the accurate determination of the sign of the lepton charges, it was important that the most accurate measurements of track curvature were performed. For this reason we did not use data taken before the installation of the Vertex Chamber in 1981. We also did not require the lepton tracks to be constrained to come from the e^+e^- annihilation point, since semileptonic decays of B and C hadrons

can occur at significant distances from their production point.

The Vertex Chamber

The Vertex Chamber (VC) was a high precision, cylindrical drift chamber which was located at the center of the detector, the beam line running along the chamber's z-axis. The inner radius of 7.6cm was defined by the beam pipe, while the outer radius was 35cm. The length of the chamber was 1.2m. It contained a total of 825 sense wires, all strung in the axial direction. These wires were arranged in two concentric bands, separated radially by a distance of 20cm, giving two measured direction vectors for each charged track. The chamber was operated with a mixture of 50% Argon, 50% Ethane at a slight overpressure. The chamber operated at a high gain, with a fully saturated gas, giving a constant drift velocity over the drift cell.

The position resolution, measured using Bhabha tracks, was 85μm at the center of a drift cell, and 100μm at the edge of the cell. This resolution was significantly degraded for tracks in multi-hadronic events due to electronic cross-talk in the VC preamplifiers. The track-reconstruction efficiency was also somewhat degraded for tracks in hadronic jets due to the double track resolution of 5mm.

The Central Drift Chamber

The Central Drift Chamber (DC) consisted of sixteen concentric layers of sense wires between an inner radius of 41cm and an outer radius of 145cm, with a length of 270cm. There were six axial layers and ten stereo layers which provided information about the z-coordinate of the track. The chamber was operated with a mixture of 50% Argon, 50% Ethane at room temperature and atmospheric pressure.

The position resolution was ~ 200μm in the x-y plane, and ~ 3mm in z. There was a total of 0.03 radiation lengths of material preceding the DC, and 0.007 radiation lengths preceding the VC. The magnetic field was 2.3kG for essentially all of the PEP5 data included in this thesis.

The combined momentum resolution of the two chambers was :

$$\frac{\delta p}{p} = \sqrt{(0.025)^2 + (0.011\,p)}$$

where the reconstructed momentum, p, is in GeV/c. The first term comes from multiple scattering in the material preceding the DC, while the second term represents the intrinsic resolution of the chambers.

For approximately $25pb^{-1}$ of the data, the Drift Chamber operated with a reduced high voltage due to excessive current draw. The tracking efficiency was somewhat reduced during this period. After the addition of a small quantity of ethanol to the gas mixture, the dark current problems were alleviated, and the chamber was returned to its full operating voltage.

The Solenoid Coil

The coil was a conventional, water-cooled, aluminum coil with an inner and outer winding which was designed to develop a uniform magnetic field of strength 4.6kG along the z-axis within the Drift Chambers. Unfortunately, the coil developed a short between the inner and outer windings, and the available field was only 2.3kG for essentially all the data used for this thesis. The total thickness of the coil was 1.4 radiation lengths.

The Liquid Argon Calorimeter[20]

The Liquid Argon Calorimeter (LA) consisted of eight planar modules arranged in an octagon around the outside of the solenoid coil. The mean radius of these modules from the center of the detector was ~ 1.8m; their length was ~ 3.6m. The modules consisted of alternating layers of lead 2mm thick and liquid Argon 3mm thick, enclosed inside an aluminum vacuum casing. Every second lead layer was made of instrumented strips kept at +3.5kV to collect the ionization electrons created by charged particles and electromagnetic showers in the Argon gaps. The other lead layers were electrically grounded. The total thickness of a calorimeter module was 14.4 radiation lengths (1.1 nuclear in-

teraction lengths) at normal incidence, and there were ~ 1.4 radiation lengths of material (mainly the solenoid coil) preceding the first readout plane.

The directions of the strips within a module alternated between being aligned parallel to the z-axis (phi-layers), perpendicular to the z-axis (theta-layers), and at 45° to the z-axis (U-layers). The phi- and theta-strips were 3.8cm wide, while the U-strips were 5.4cm wide. The readout planes were ganged together as follows :

F Planes Nine of the phi-planes from the front, middle and back sections of a module were ganged together to form three separate readout layers, F1 (front), F2 (middle), and F3 (back).

T Planes Six of the theta-planes from the front and middle sections were ganged into two separate readout layers, T1 (front) and T2 (middle).

U Planes The three U-planes from the front half of the module were ganged together to form the U1 layer.

Liquid Argon Calorimeter ganging scheme

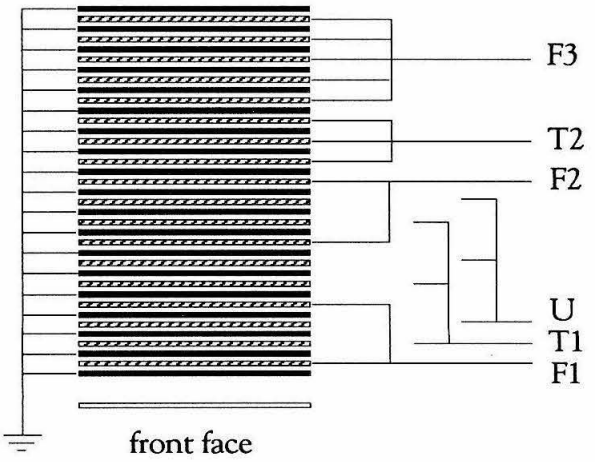

Figure 2. 2

The energy resolution of the system for Bhabhas was measured to be (E in GeV):

$$\frac{\sigma(E)}{E} = \frac{15\%}{\sqrt{E}}$$

The Muon System

The Muon System was a four layer, planar hadron absorber made of steel interspersed with proportional chambers. It covered the top, bottom, right and left sides of the detector to provide coverage of ~ 45% of the total solid angle. Hadrons were expected to range out in the steel due to inelastic nuclear interactions, while muons with momenta greater than 1.8 GeV/c were expected to penetrate, leaving associated hits in all four layers of proportional chambers. The average thicknesses of the layers of absorber are shown in Table 2. 1, where d is the thickness in cm, and l is the thickness in nuclear interaction lengths. The row "before 1" refers to the material preceding the first layer of absorber — mainly the LA calorimeter and the solenoid coil.

Hadron absorber thickness in Muon System

	East		Top		West		Bottom	
layer	*d*	*l*	*d*	*l*	*d*	*l*	*d*	*l*
before 1	19.4	1.17	19.4	1.17	19.4	1.17	19.4	1.17
1	23.1	1.38	23.1	1.38	23.1	1.38	23.1	1.38
2	23.4	1.40	23.4	1.40	23.4	1.40	23.4	1.40
3	31.0	1.85	30.4	1.81	31.0	1.85	31.0	1.85
4	24.9	1.49	23.4	1.40	24.9	1.49	31.0	1.85
total	**121.8**	**7.28**	**119.7**	**7.16**	**121.8**	**7.28**	**127.9**	**7.65**

Table 2. 1

The tubes in the innermost layer are oriented perpendicular to the beam direction to measure the polar coordinate of the track, while the tubes in the outer three layers are oriented parallel to the beam direction to measure the azimuthal coordinate. The pro-

portional chambers were constructed of aluminum extrusions which accommodated eight individual channels, as shown in Figure 2. 3.

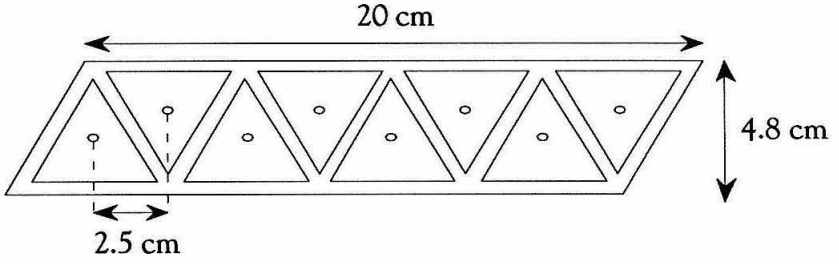

Figure 2. 3

The wires in each module were separated by 2.5cm to match the expected multiple scattering between layers. The chambers were operated in a high-gain mode with a mixture of 95% argon and 5% carbon dioxide. The 45μm diameter, gold-plated tungsten wires were kept at an operating voltage of +2kV. The signal from each channel was discriminated at a 2mV threshold, and fed into a shift register; the shift registers being serially read out when an event trigger was received. There was a total of 3264 wires in the system.

Other systems

There were several other systems which did not directly contribute to this analysis :

Time of Flight system

The TOF system was located between the Drift Chamber and the solenoid coil. It consisted of 48 slabs of plastic scintillator 1.5m long, 20cm wide and 2.5cm thick, with phototubes at both ends. It was used in the charged particle trigger, for rejection of cosmic ray events, and for electron-pion-kaon-proton separation for tracks with momenta of less than ~ 1 GeV/c. The measured average timing resolution of the system for Bhabha tracks was ~ 350ps, being better for early data, and worse for later data as the scintillator became damaged by radiation .

Endcap Calorimeter

At both ends of the Drift Chamber, covering the range of polar angles between 15°–40°, was a lead/proportional tube electromagnetic calorimeter. The total thickness was 2.5 radiation lengths, and the energy resolution for electromagnetic showers, measured using radiative Bhabhas (E in GeV), was :

$$\frac{\sigma(E)}{E} = \frac{50\%}{\sqrt{E}}$$

Small Angle Tagger system

The SAT system was used to detect the presence of particles at very small angles to the beam direction. It covered the angular region 20-80mrad and was used for determining the luminosity using small angle Bhabhas, and for tagging beam particles at small angles from two-photon events.

The upgraded detector

After the PEP5 data taking was completed in 1984, the Mark II detector was upgraded in preparation for installation in the Stanford Linear Collider. In order to check the performance of the new detector elements, ~ 25 pb^{-1} of data were taken in the PEP ring between September 1986 and February 1987. This data sample became known as the PEP Upgrade sample. Unfortunately, the first 10 pb^{-1} of data contained no muon system information due to a timing problem in the data acquisition system.

The new detector elements were :

Vertex Chamber A new vertex chamber[21] was constructed for the upgrade run. It consisted of six concentric layers of single-wire drift cells (straws) with inner and outer radii of 9.5 and 14.8cm, respectively. There was a total of 552 wires, and the mean position resolution across a cell was ~ 90μm. The chamber was 1.2% of a radiation length thick for particles at normal incidence.

Drift Chamber The new chamber consisted of 12 concentric layers of jet cells, each cell containing six sense wires. This jet cell design enabled twelve direction vectors to be formed for each charged track, one for each layer. The track finding was then accomplished by finding clusters of vectors in a rho-phi plane, where rho and phi were the estimated track curvature and the extrapolated azimuthal coordinate at the IP for each vector. This chamber had substantially improved momentum and two-track resolutions over the PEP5 chamber. It also provided a measurement of dE/dx with a resolution of ~ 8% for charged tracks, providing limited discrimination between electrons, pions, kaons and protons for momenta between 1 and 10 GeV/c. Unfortunately, less than 20% of the dE/dx system was implemented for the Upgrade run. The measured momentum resolution for the combined drift chambers was given by :

$$\frac{\delta p}{p} = \sqrt{(0.014)^2 + (0.005\,p)}$$

Solenoid Coil A new coil was made to replace the shorted PEP5 coil. It was a conventional, water-cooled aluminum coil 1.3 radiation length thick and provided a magnetic field strength of 4.5kG.

TOF system A new Time of Flight system was constructed with improved timing resolution due to thicker scintillator (4.5cm) and faster phototubes. The measured timing resolution was ~ 220ps for Bhabhas, and ~ 290ps for hadronic tracks.

Because the upgrade data sample represented less than 10% of the PEP5 data sample, we did not consider the two samples separately. The LA calorimeter and muon system were not changed in the upgrade, and, to first order, the lepton identification properties of the detector were not substantially different.

Chapter 3

Lepton Identification

LEPTON identification plays a crucial role in this thesis; it is the means by which we can infer the decay of bottom quarks, and the charges of these quarks. In this chapter we discuss in detail how leptons are identified by the Mark II detector, and how the backgrounds to lepton identification are estimated. A detailed description of lepton identification using the Mark II can be found in reference [22], which was the source for most of the material presented in this chapter.

Electron identification

Electrons passing through material tend to lose kinetic energy more rapidly than other charged particles†. This is primarily due to the small mass of the electron, which leads to more rapid ionization losses and substantial *Bremsstrahlung* (where an electron radiates energy as it decelerates). The natural scale length for the depth to which an electron will penetrate material is the *radiation length*. This is defined as the average distance over which an high energy electron (≥ 1 GeV) loses all but a fraction $1/e$ of its energy, and depends on various properties of the material traversed such as the atomic number and the density.

Other charged particles lose energy through ionization and, in the case of hadrons, through nuclear interactions. The rates of such energy losses are substantially smaller than for Bremsstrahlung, hence electrons can be distinguished from other charged particles by their range in material.

† These statements apply to electron energies between a few hundred MeV, and a few tens of GeV.

In e^+e^- annihilation experiments, it is desirable to measure the energy depositions of all the charged and neutral particles in the hadronic "jets," to provide particle identification information. The material used to "range-out" the electrons (the Calorimeter) should therefore be active in order to measure the pattern of energy deposition, and the total energy deposited. It should also have lateral segmentation to be able to distinguish between the individual energy deposits, and segmentation in depth to measure the rate of longitudinal energy deposition. Finally, to provide an accurate measurement of the electron's energy, it must be thick enough to contain essentially all of the electron "shower."

Implementation

The Mark II LA Calorimeter, described in Chapter 2, is a total of 14.4 radiation lengths thick, providing essentially total containment of all but the highest energy electron showers.† The readout strips are between 3.8 and 5.4cm wide, providing a reasonable compromise between fine segmentation and a feasible data acquisition system. It is also segmented in depth, providing measurements of energy deposition in the front, middle, and back sections. (The Calorimeter was originally designed for e^+e^- annihilation at 5.2 GeV, and is currently taking data at the Z^0 resonance at 91.1 GeV ; an indication that the compromise made was probably reasonable for e^+e^- annihilation at 29 GeV.)

The algorithm used to distinguish electron showers from the energy depositions of other charged and neutral particles has been described in several previous publications[22]. The idea was to measure the energy deposition at several depths within the Calorimeter within a small search region centered on the extrapolation of the track from the Drift Chamber. These energy depositions were then tested against the expected depositions from an electron with the same momentum as the candidate track. If any of the depositions were less than those expected for an electron shower, the candidate track failed to be identified as an electron.

† Electrons with energies less than a few hundred MeV cannot be identified reliably by the Mark II Calorimeter because of the finite energy losses in the material preceding it.

The procedure was as follows :

i) The Drift Chamber tracking information was used to obtain the expected position and angle of the track at the F1, F2, T and U layers.

ii) A search region was calculated about the expected position in each layer. Because of the ganging scheme geometry (see Figure 2. 2), the search region size depends on the angle that the track makes with the normal to the Calorimeter, and the differences in depth of the strips within a ganged group. Specifically :

$$W_{search} = W_{shower} + W_{gang} \times |\tan \delta|$$

where W_{search} is the size of the search region, W_{shower} reflects the width of a typical electron shower (~ 3cm), W_{gang} depends on the ganged group used, and δ is the angle the track makes with the normal of the Calorimeter. The values used for W_{shower} for the F1, F2 and T1 layers were 0.75 units; the U layer value was 0.70 units. The values of W_{gang} were 0.9 units for the F1 and F2 layers, and 1.5 units for the T1 and U layers. The units used were the strip widths. If the center of a strip was within the search region, the energy associated with that strip was associated with the incident track.

iii) Four distinct energy sums were formed from the energies associated with the incident track, namely E_F, E_T, E_U and E_{front}. E_F is the sum of E_{F1} and E_{F2} , while E_{front} is the sum of E_F, E_T and E_U. From studies of known sources of electrons, an "electron-like" track would satisfy :

$$\begin{aligned} E_F &> \alpha_F \times p & (\alpha_F &= 0.14) \\ E_T &> \alpha_T \times p & (\alpha_T &= 0.10) \\ E_U &> \alpha_U \times p & (\alpha_U &= 0.10) \\ E_{front} &> \alpha_{front} \times p & \left(\alpha_{front} = \begin{matrix} 0.50, & p < 4 \\ 0.40, & p > 4 \end{matrix}\right) \end{aligned}$$

where p is the momentum of the candidate track. The α parameters were chosen to optimize the electron identification efficiency while maintaining good rejection of non-electron tracks.

iv) We can form the variable E_{min} to be the minimum value of the four quantities E_F / α_F, E_T / α_T, E_U / α_U and $E_{front} / \alpha_{front}$; the criterion for a track to be identified as an electron, as given above, is then simply $E_{min} / p > 1$.

In practice, in order to maximize the rejection of non-electronic tracks (at the expense of a slight reduction in the electron identification efficiency) the criterion for electron identification was chosen to be $E_{min} / p > 1.1$.

Electron Identification efficiency

Electron identification efficiency

p (GeV/c)	*data*	*Monte Carlo*
1.0 - 1.5	0.71	0.73
1.5 - 2.0	0.75	0.77
2.0 - 2.5	0.88	0.90
2.5 - 3.0	0.89	0.92
3.0 - 3.5	0.90	0.94
3.5 - 4.0	0.90	0.94
4.0 - 4.5	0.91	0.94
4.5 - 5.0	0.91	0.94
5.0 - 5.5	0.91	0.94
5.5 - 6.0	0.91	0.95
> 6.0	0.92	0.95

Table 3. 1

The electron identification efficiency has been measured[23] by using sources of known electrons, namely Bhabha electrons, radiative Bhabha events and two photon events of the type $e^+e^- \rightarrow e^+e^- e^+e^-$. The systematic error associated with these efficiencies is of order 3% due to uncertainties in tracking errors and the overlap of neutral energy in multi-hadronic events. The efficiency as measured by the Monte Carlo is consistently higher than that measured in the data.

In this thesis the exact values of the lepton identification efficiencies are relatively unimportant since the efficiencies are expected to be the same for both positive and negative leptons. In Chapter 5, we use the values of the lepton identification efficiencies to extract the semileptonic branching ratios for B and C hadron decays, but since these efficiencies only affect the overall normalization of the lepton sample to first order, they do not affect the mixing results.

Decay backgrounds

What we refer to as "Decay" backgrounds are electrons which do not come from semileptonic decays of C or B quarks. These electrons come from photon conversions in the material of the detector (mainly in the beam pipe and the outer wall of the Vertex Chamber) and Dalitz decays of π^0s (*i.e.* $\pi^0 \rightarrow e^+e^-\gamma$). A pair finding algorithm[22] was used to identify and remove these electrons. Using the Monte Carlo, the efficiency with which these pairs was found was estimated to be about 70%. The number of remaining tracks were estimated using the Monte Carlo. In general, these decay electrons tend to have low momenta and to be within the body of the hadronic jets (having low p_t).

Misidentification backgrounds

The majority of the backgrounds to electron identification are charged pions, kaons and protons which overlap with energy deposits from photons or other tracks, or which have an inelastic nuclear interaction early in the calorimeter. We refer to these as *misidentification* backgrounds. Because of the lack of an adequate hadronic interaction simulator in the Monte Carlo for the Calorimeter, the probability for a given track to be misidentified as an electron has been estimated using sources of known hadrons[22]. This misidentification probability depends on many factors. The most important of these are the momentum of the incident track and the isolation of this track from the hadronic jet. We therefore have parametrized the misidentification probability in terms of the momentum, p, and transverse momentum, p_t, of the incident track. The misidentification probability depends strongly on the amount of energy associated with the candidate track due to overlap with other charged and neutral tracks.

The misidentification probabilities were determined[22] by studies of sources of known pions from SPEAR data and pion test beam data. The effects of track overlap were estimated by a "track-flipping" procedure in which candidate tracks were rotated azimuthally by 180°. Because of the back-to-back structure of two-jet events at PEP energies, the rotated track was usually projected into the opposite jet. The energy associated with this fictitious track should be the "overlap energy," if one corrects for the higher energy

density in the jet containing the flipped track. The misidentification probabilities were originally parametrized in terms of the track momentum and the momentum transverse to the event thrust axis. Since our definition of p_t was different, we reparametrized the probabilities in terms of p and p_t. We list these per-track misidentification probabilities in Table 3. 2. We assume that pions, kaons and protons have equal misidentification probabilities, and that these probabilities are the same for the positive and negative hadrons.

Hadron→ electron misidentification probabilities (%)

p (GeV/c)	0.0 - 0.5	0.5 - 1.0	1.0 - 1.5	> 1.5 p_t (GeV/c)
1.0 - 1.5	1.64	0.95	0.55	0.55
1.5 - 2.0	1.57	0.94	0.60	0.60
2.0 - 2.5	1.20	0.89	0.56	0.56
2.5 - 3.0	0.97	0.67	0.53	0.53
3.0 - 3.5	0.77	0.60	0.48	0.48
3.5 - 4.0	0.64	0.52	0.45	0.45
4.0 - 4.5	0.57	0.50	0.45	0.45
4.5 - 5.0	0.54	0.48	0.45	0.45
5.0 - 5.5	0.52	0.48	0.45	0.45
5.5 - 6.0	0.48	0.45	0.45	0.45
> 6.0	0.45	0.45	0.43	0.43

Table 3. 2

These misidentification probabilities have been checked using sources of known pions from the data. These included phi decays from SPEAR, three-prong decays of taus and K^0 decays to two charged pions. Within the statistical and systematic errors associated with these sources of pions, there was good agreement with the estimated per-track misidentification probabilities. The systematic error associated with the probabilities in Table 3. 2 is ~ 40%.

Muon identification

Like electrons, muons are distinguished from other charged particles by their interaction with matter. In the case of the muon, the range in material is relatively large since its mass is sufficient to make Bremsstrahlung very unlikely, and, being a lepton, it cannot undergo strong nuclear interactions. At the energies we are considering, the dominant energy loss mechanism is ionization of the material the muon is passing through. Muons can therefore be distinguished from other charged particles by their ability to penetrate material; all other charged particles have a shorter effective range than the muon.

Implementation

The Mark II detector has a four layer, steel/proportional-tube hadron absorber to identify muons, as described in Chapter 2. Because of the thickness of the absorber, averaging over seven nuclear interaction lengths, more than 99.9% of hadrons are expected to undergo a nuclear interaction before the outermost layer. However, muons with momenta above about 1.8 GeV/c are expected to penetrate all four layers of absorber, leaving hits in the four layers of proportional chambers. The Muon System covers ~ 45% of the total solid angle subtended at the interaction point.

The muon identification algorithm uses the Drift Chamber tracking information to project the candidate track into the muon system, and calculates the expected position of the track at each of the four proportional chamber layers. The total amount of material preceding each layer is then estimated, and the expected R.M.S. error in the position of the track at each layer is calculated. This error is due to multiple scattering in the material traversed by the candidate muon, the expected Drift Chamber tracking extrapolation error and the intrinsic resolution of the muon chambers. Since the angular deviation due to multiple scattering is approximately proportional to the inverse of the track momentum, multiple scattering dominates the position error for momenta less than ~ 5 GeV/c. The Drift Chamber track extrapolation errors give rise to the position errors evaluated at each plane which are given in Table 3. 3†.

† The Upgrade Drift Chamber had substantially smaller track extrapolation errors than those listed in Table 3. 3.

DC track extrapolation errors (cm)				
layer	*East*	*Top*	*West*	*Bottom*
1	3.0	2.0	3.0	2.0
2	2.0	1.5	2.0	1.5
3	2.3	1.8	2.3	1.8
4	2.6	2.1	2.6	2.1

Table 3. 3

Because of the triangular geometry of the proportional chambers, a single track passing through the chambers could leave hits in two adjacent chambers. In this case, the coordinate of the track, as measured by the proportional chambers, was taken as being the average of the coordinates of the two wires with hits. If only a single wire registered a hit, then the coordinate of that wire was used as the measured coordinate of the track. Because the proportional chamber wires were 2.5cm apart, the intrinsic position resolution was ~ 0.75cm. The multiple scattering error, DC extrapolation error and the muon chamber intrinsic resolution were combined in quadrature to obtain the expected R.M.S. error in the position of the track at each of the four layers. Muon candidates were then required to have a proportional chamber hit in each of the four layers within a search region equal to three times the expected R.M.S. position error on either side of the expected track position, as shown in Figure 3. 1.

Muon identification efficiency

The efficiency for identifying muons has been measured by using sources of known muons from the data: Cosmic rays, mu-pair and radiative mu-pair events, and two-photon events of the type $e^+e^- \rightarrow e^+e^- \mu^+\mu^-$ were used to obtain the identification efficiencies shown in Table 3. 4. These identification efficiencies have errors of ~ 3%. The Monte Carlo efficiencies are systematically higher than those measured in the data because the simulation overestimated the per-plane efficiency by approximately 1.5%.

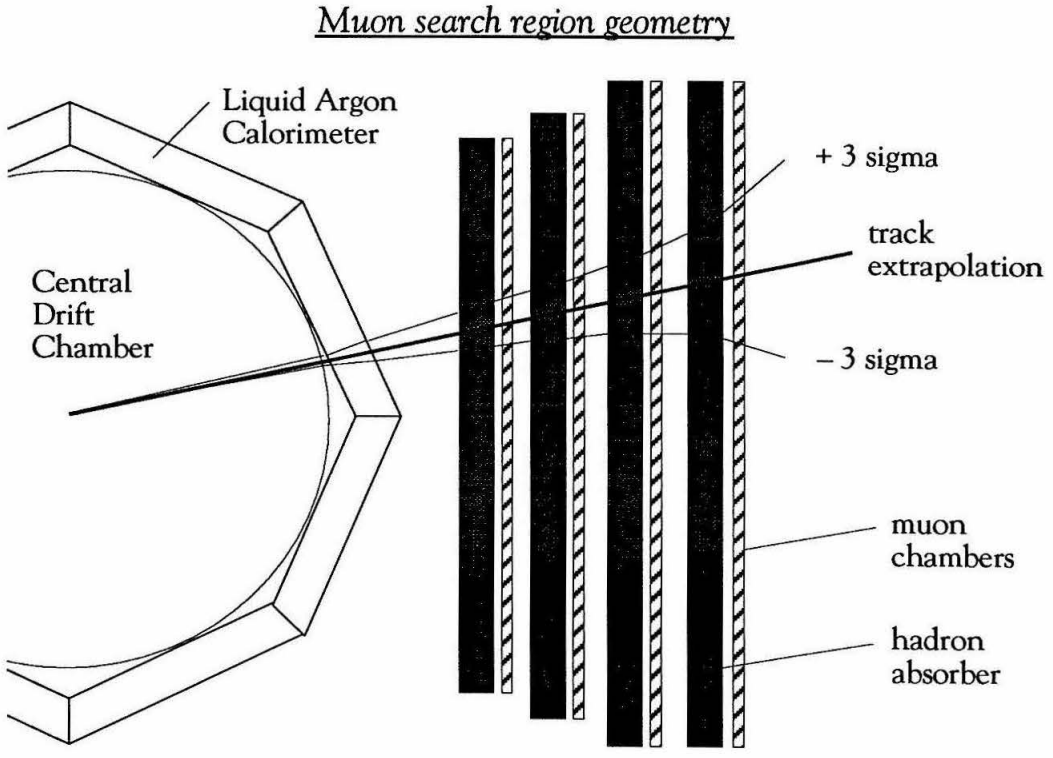

Figure 3. 1

Decay backgrounds

Charged pions and kaons are unstable and decay to produce muons (and, to a much smaller extent, electrons) and their associated neutrinos. The proper lifetimes for pion and kaon decay to muons are 26ns and 19ns, respectively. The probability for a relativistic particle with mass m (GeV/c^2), momentum p (GeV/c) and proper lifetime t (seconds) to decay before it has traveled a distance l (meters) is given by :

$$Prob\ (< l) = 1 - exp\left(-\frac{ml}{pct}\right)$$

Muon identification efficiency		
p (GeV/c)	*data*	*Monte Carlo*
1.5 - 2.0	0.46	0.48
2.0 - 3.0	0.82	0.86
3.0 - 4.0	0.87	0.91
4.0 - 5.0	0.88	0.92
5.0 - 6.0	0.90	0.93
> 6.0	0.91	0.95

Table 3. 4

The fraction of pions and kaons that decay to muons within the Drift Chamber is then approximately :

$$\pi \rightarrow \mu\nu \quad Prob\ (l < 1.6m) \approx \frac{0.029}{p}$$

$$K \rightarrow \mu\nu \quad Prob\ (l < 1.6m) \approx \frac{0.136}{p}$$

In principle, this represents a serious background to the prompt muon signal due to the much larger number of pions and kaons than prompt muons in hadronic events. However, in practice, the momentum of the decay muon is somewhat less than that of the parent hadron, and therefore many of the muons do not penetrate the hadron absorber. Also, if the decay takes place within the the main body of the drift chamber, the decay track and parent track may be sufficiently acollinear that the track reconstruction code may reconstruct the vertex, or the combined parent-daughter track may be rejected due to a poor track fit. The fraction of parent-daughter tracks which are reconstructed as a single track with a reasonable track fit is a complicated function of the Drift Chamber performance, which can only be addressed by a detailed Monte Carlo simulation of pion and Kaon decays in the detector. Such effects were included in our simulation of hadronic events produced by the Monte Carlo, which we used to predict the number of "decay" muons in our final event sample.

Misidentification backgrounds

We have seen in Chapter 2 that a particle has to traverse more than seven nuclear interaction lengths of material in order to reach the fourth muon system layer. One might then naïvely calculate that the probability of a hadron being misidentified as a muon as :

$$Prob\left(H \rightarrow \mu\right) \approx 1 - exp\left(-7\right)$$
$$\approx 0.09\ \%$$

This would be a serious underestimate for several reasons :

- It assumes that the absorber is homogeneous. In practice, if the absorber is segmented, the hadron (a charged pion or kaon) has a greater probability of decaying to a penetrating muon.
- It does not take into account the particle type or charge.
- It neglects the possibility of hadronic punchthrough†. It also neglects the possibility that hits from adjacent tracks could be assigned incorrectly to the candidate track.

Although the inelastic nuclear interaction cross sections for pions, kaons and protons are different, we do not distinguish between them in this thesis due to our inability to differentiate between these particle types in the data. The difference in the cross sections for positive and negative particles is accessible, however. The inelastic hadron-proton cross sections for positive and negative pions (which constitute about 70% of all the hadrons produced) are expected to be approximately the same. However, the K^+–proton inelastic cross section is almost half that of the K^-–proton cross section; and the proton-proton inelastic cross section is also about half the anti-proton–proton cross section. We might therefore expect to see a charge asymmetry in the number of hadrons which are misidentified as muons.

In order to estimate the extent of this charge asymmetry we used an hadronic interaction simulation program[24]. Although the charge asymmetry is observable in the data,

† "Punchthrough" is the process where a hadron, or the shower produced from a hadronic interaction, penetrates all four layers of the muon system, and the resulting pattern of associated muon chamber hits satisfies the muon identification algorithm.

the effect is considerably smaller than the overall systematic error which we associate with the estimation of the hadronic misidentification probabilities, ~ 35%. Also, even though there is a small charge dependence to the hadronic misidentification, this does not necessarily introduce a correlation between the charges of leptons in opposite jets (unless they are both misidentified hadrons). Even in this case, the error made in neglecting this effect is totally negligible in comparison to other systematic errors.

The inelastic nuclear interaction cross section is essentially independent of momentum over the range we are considering. This means that the depth of the primary interaction point in the calorimeter/hadron absorber is not a function of the track momentum. If one were able to determine this point of initial interaction (by having a finely grained hadron calorimeter, for example) then the "punchthrough probability" would also be independent of momentum. However, the Mark II muon system does not have the capability to identify and reject the tracks of particles from an inelastic nuclear interaction. Therefore, as the number and energy of such hadronic "secondaries" increases due to higher incident hadron momenta, the apparent punchthrough will increase.

In the center of an hadronic jet, a track may have muon chamber hits associated with it which originated from another track. This effect will give rise to a higher punchthrough probability for tracks which are not isolated (which generally have low p_t), than those which are isolated from jets.

Determination of the hadron → muon misidentification probabilities

The probability for a hadron to be misidentified as a muon was estimated in two ways. The first method involved performing a fit to the pattern of hits in the muon chambers for tracks which failed the muon identification algorithm. The fit parameters were the punchthrough probabilities to the first three muon system layers. The punchthrough probability to the fourth layer was then obtained by extrapolation. The second method was to use the hadronic interaction Monte Carlo[24]. The results from these two independent methods gave good agreement. As a cross-check, we used a source of known pions from the data, namely the three prong decays of taus. These methods are

described in more detail below.

i) Fitting the muon chamber data

The hits which have been associated with a candidate muon track are stored as a pattern of four bits, indicating whether a hit was found within the three standard deviation search region about the track's position in each of the four layers. Since we required an identified muon to have an associated hit in all four layers, the value of this bit pattern for a valid muon would be 15 (*i.e.*, 1111_2). Because the muon identification efficiency was reasonably high (~ 85-90%), tracks with an associated hit pattern of less than 15 are almost exclusively hadrons. We therefore used this sample of "known hadrons" to measure the fraction of all hadrons which punched through to layers 1, 2 and 3 (layer 4 was "contaminated" by valid muons).

In the absence of any random noise in the muon chambers, one would expect the hit patterns for punchthrough to layers 1, 2 and 3 to be 0001, 0011 and 0111, respectively. In fact, for certain periods of running there was a significant amount of noise in the chambers due to beam-related synchrotron radiation. The presence of random noise changed the hit patterns, producing a range of values between 0001 and 1111. It was the distribution of these values which was fitted, taking random hits into account. The three variables in the fit were the probabilities that a hadron punched through to layers 1, 2 and 3, respectively. To obtain the momentum and p_t dependence of these punchthrough probabilities, separate fits were done on samples of tracks binned in p and p_t. For each p and p_t bin we obtained the fitted values of the per track punchthrough probabilities to the first three layers. We then assumed that the punchthrough probability followed a decaying exponential distribution given by :

$$P(p, p_t) = exp\left(-\frac{d}{\lambda(p, p_t)}\right)$$

where $P(p, p_t)$ is the per track punchthrough probability, d is the total amount of material traversed by the track and $\lambda(p, p_t)$ is the "decay constant" as a function of momentum and transverse momentum. A graph of the punchthrough probabilities as a

function of the amount of material traversed is shown for three different values of momentum in Figure 3. 2.

Hadronic punchthrough probabilities

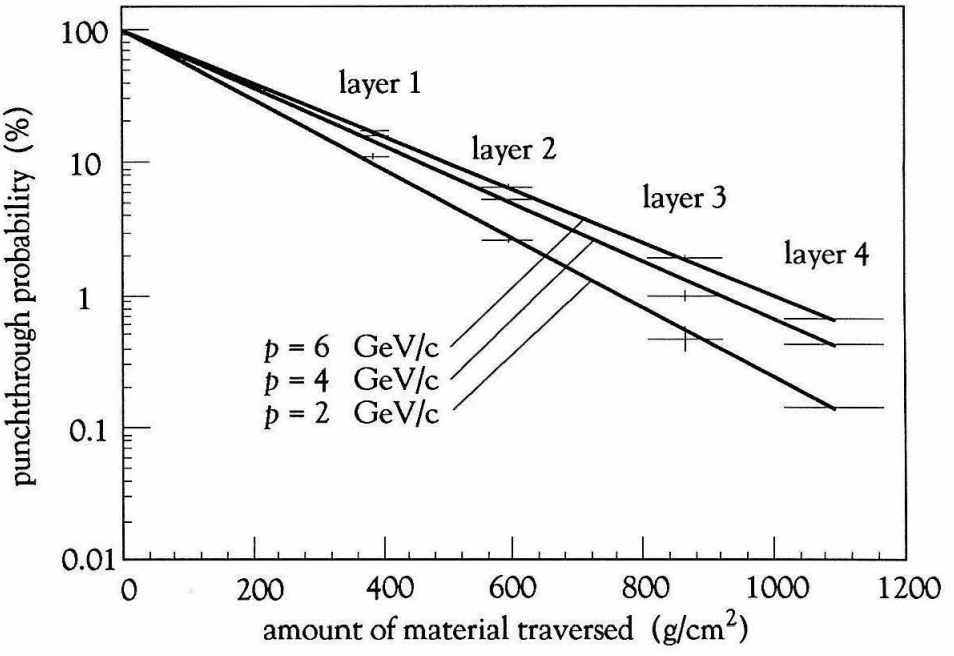

Figure 3. 2

The value of the punchthrough at layer 4 was inferred by extrapolation. The errors in the amount of material traversed, shown as the horizontal error bars, were due to the different angles of incidence of the candidate tracks.

ii) The hadronic interaction Monte Carlo

We used the Monte Carlo to generate a large sample of hadronic tracks which were within the muon system acceptance. The fraction of these tracks which punched through to layers 1, 2 and 3 (*i.e.*, which had hit patterns of 0001, 0011 and 0111) as a

function of momentum and transverse momentum were then compared with the data. The Monte Carlo included the effects of random noise in the proportional chambers, and the Drift Chamber tracking errors. As shown in Figure 3. 3, there is good agreement between the predictions of the Monte Carlo and the hadronic punchthrough observed in the data.

The variable p_t / p is a measure of the angular isolation of a track from the other charged tracks in the event. Because of the momentum dependence of the punchthrough probability, the dependence on the track isolation is clearer when shown as a function of this dimensionless variable. The good agreement seen for the punchthrough probabilities for the first three layers gives confidence in the prediction for the punchthrough to the fourth layer.

The combined values of the misidentification probabilities using the fit to the hit-pattern distributions and the Monte Carlo are listed in Table 3. 5. The estimated systematic error on these probabilities is ~ 35%.

We have checked these probabilities by using a source of known pions, namely the three-prong decays of tau leptons produced in tau pair events[23] :

$$\tau^- \rightarrow \pi^+ \pi^- \pi^- \nu_\tau$$

These pions tend to have fewer "overlapping" hits in the muon chambers due to adjacent tracks because of the substantially smaller number of tracks in the events. Also, the total number of such events was sufficiently small that the resulting misidentification probability had a substantial statistical error. The estimated misidentification probability, averaged over all values of the pion momentum and transverse momentum, was determined to be $0.32 \pm 0.07\%$, in good agreement with the values in Table 3. 5.

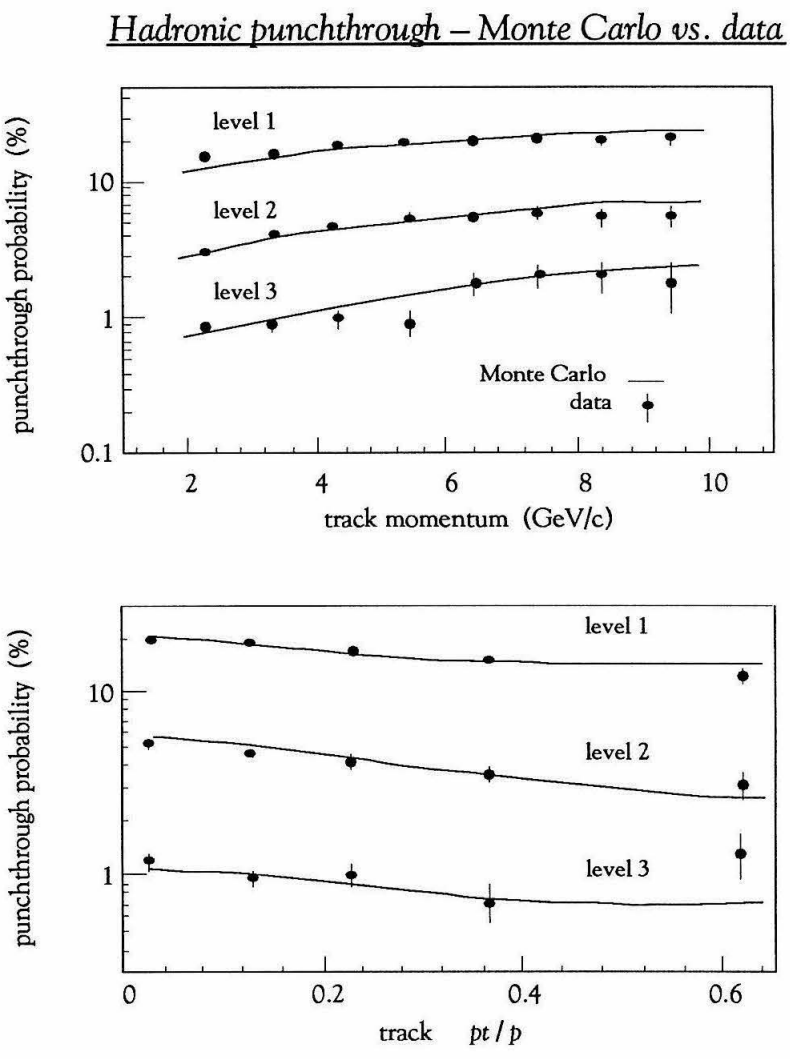
Hadronic punchthrough – Monte Carlo vs. data
punchthrough probability (%)
level 1
level 2
level 3
Monte Carlo
data
track momentum (GeV/c)
punchthrough probability (%)
level 1
level 2
level 3
track pt / p

Figure 3. 3

Hadron → muon misidentification probabilities (%)

p (GeV/c)	0.0 - 0.5	0.5 - 1.0	1.0 - 1.5	> 1.5	p_t (GeV/c)
1.5 - 2.0	0.45	0.33	0.26	0.18	
2.0 - 2.5	0.47	0.36	0.28	0.20	
2.5 - 3.0	0.51	0.47	0.30	0.29	
3.0 - 3.5	0.55	0.49	0.32	0.31	
3.5 - 4.0	0.62	0.52	0.45	0.42	
4.0 - 4.5	0.69	0.56	0.53	0.48	
4.5 - 5.0	0.79	0.68	0.59	0.56	
5.0 - 5.5	0.95	0.77	0.63	0.60	
5.5 - 6.0	0.98	0.80	0.68	0.65	
> 6.0	1.02	0.88	0.75	0.73	

Table 3. 5

Chapter 4

Event Selection

In this chapter we describe the event selection cuts used to obtain a pure sample of multi-hadronic events containing leptons from the semileptonic decays of heavy quarks.

Multi-hadronic events† are those in which the initial electron and positron annihilate to produce a quark-antiquark pair via the one-photon exchange diagram in Figure 1. 1. Events of this type are generally distinguished from other events by the relatively large number of tracks present in the detector. Typical charged track multiplicities for charm and bottom events have been measured by the Mark II[25] to be ~ 13 and ~ 16, respectively. Other events present in the data are mainly Bhabhas, mu-pairs, tau-pairs, two-photon events and beam-gas events. All these event types generally have small numbers of tracks, or the candidate leptons are very isolated from other tracks, and therefore it is relatively straightforward to isolate a pure sample of multi-hadronic events.

Hadronic event selection

Keeping in mind that hadronic events generally have many charged tracks which come from the interaction point, that these tracks are usually clustered together in jets, and that most of the available energy is visible in the detector, we defined the event selection cuts listed in Table 4. 1.

† Often referred to simply as *hadronic* events.

Hadronic event selection cuts

i) At least 5 charged tracks which pass within 4cm radially, and 6 cm axially, from the interaction point. None of these tracks should be from identified photon conversions.

ii) Scalar sum of momenta of charged particles > 3.0 GeV/c, and total charged + neutral energy > 7.5 GeV/c.

iii) z-component of thrust axis be smaller in magnitude than 0.7.

iv) At least one charged particle cluster found in the event.

A total of 81,744 events passed these cuts, 76,738 being in the PEP-5 sample and 5,006 in the Upgrade sample.

Table 4. 1

Using cut *i)* we rejected events with small numbers of charged tracks, and those in which the primary interaction point was not at the center of the detector. With cut *ii)* we rejected events in which there was a large amount of energy missing. Using cut *iii)* we required the event to be well contained within the detector. Since the acceptances of the Calorimeter and Muon System were essentially zero for tracks with a small polar angle, this cut did not strongly affect the selection of events containing leptons. With cut *iv)* we rejected events in which there were not enough tracks to form a charged particle cluster. If we could not have constructed such a cluster, the definition of the transverse momentum for candidate leptons would have been meaningless.

Leptonic event selection

The criteria used to identify leptons have been discussed in Chapter 3. We list in Table 4. 2 the additional requirements made in order to isolate the two samples of hadronic events used in the inclusive lepton analysis in Chapter 5. The single lepton sam-

ple was required to have one, and only one, identified lepton. The dilepton sample was required to have two, and only two, identified leptons.

Single lepton event cuts	*Dilepton event cuts*
i) Lepton p < 9 GeV/c.	*i)* Event rejected if either lepton has p > 7.5 GeV/c *and* p_t > 3.5 GeV/c.
ii) Lepton p_t < 3.5 GeV/c.	*ii)* Leptons separated by > 90°.
iii) A charged cluster found within 90° of the lepton.	

Table 4. 2

These cuts were chosen to reduce the number of events which contained a high momentum lepton which was very isolated from other tracks in the event, typical of the two-photon and tau pair backgrounds, described below. They remove ~ 14% of the single lepton events which contain an electron from B-primary decay, and ~ 16% of the single lepton events containing a B-primary muon. They also remove ~ 5% of dilepton events in which both leptons come from B-primary decays.

After all cuts there were 6,108 candidate electrons, and 1,568 candidate muons in the single lepton sample; and 191 electron-electron, 117 electron-muon, and 23 muon-muon events in the dilepton sample.

Backgrounds: *two-photon events*

The classes of two-photon processes present in the data are shown in Figure 4. 1.

In the "annihilation", "bremsstrahlung" and "multi-peripheral" classes, one or both of the initial beam particles may be scattered into the detector. These scattered electrons and positrons will generally have high momenta, and will tend to be isolated from the

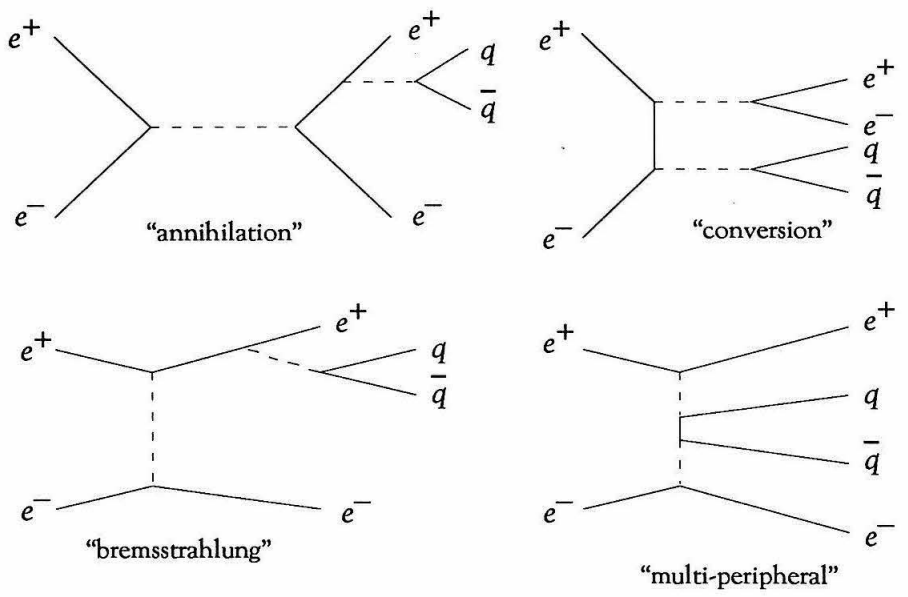

Figure 4. 1

other tracks in the event, and are therefore similar to the leptons produced from B decays. In practice, two-photon events are a more serious background to events in the one-lepton sample than to events in the two-lepton sample. In the situation where the $q\bar{q}$ pairs are either $b\bar{b}$ or $c\bar{c}$ pairs, there may be leptons present from semileptonic decays of B or C hadrons (although the center of mass energy at which these pairs would be produced is very much less than 29 GeV). There are also misidentification and decay backgrounds to lepton identification from the hadrons present in the $q\bar{q}$ jets.

In order to estimate the number of two-photon events which passed the event selection cuts, we used a Monte Carlo[26] which contained the complete lowest order calculations for two-photon produced four lepton final states. The lepton pair produced by the photon conversion or fusion was replaced by a quark-antiquark pair which were fragmented according to the Lund second order matrix element scheme, described in Appendix A.

The numbers of two-photon events passing the event selection cuts, as determined by the Monte Carlo, are given in Table 4. 3. These events are almost exclusively in the electron-electron and electron-muon classes. The estimated normalization error on the cross sections is ~ 20%. The two-photon contamination is therefore 0.3% of the hadronic sample, 0.9% of the single lepton sample, and 0.4% of the dilepton sample.

Two-photon events passing cuts

event type	*cross section (nb)*	*number in hadronic sample*	*number in one lepton sample*	*number in two lepton sample*
$ee\,u\bar{u}$	7.48 ± 1.50	136.8	37.0	0.10
$ee\,d\bar{d}$	1.55 ± 0.31	16.5	5.6	0.14
$ee\,s\bar{s}$	1.13 ± 0.22	20.2	4.3	0.18
$ee\,c\bar{c}$	1.44 ± 0.29	90.7	21.7	0.89
$ee\,b\bar{b}$	0.02 ± 0.004	3.0	1.5	0.12
total	$\mathbf{11.62 \pm 2.3}$	$\mathbf{267 \pm 53}$	$\mathbf{70 \pm 14}$	$\mathbf{1.4 \pm 0.3}$

Table 4. 3

Backgrounds: *tau pair events*

Events in which a pair of tau leptons are produced can constitute a background to the hadronic event sample since each tau can, in principle, decay to three or more charged tracks. In practice, the vast majority of tau pair events result in fewer than five charged tracks in the detector. The events which pass our hadronic event selection cuts, listed in Table 4. 1, contain exclusively pion and kaon tracks, since the only decays of taus to muons and electrons result in a single charged track in a given "jet." Therefore, the "leptons" in these events are all misidentified hadrons, or decay leptons, described in Chapter 3. The probability of an event containing *two* misidentified hadrons or decay leptons is very small, hence these events hardly contribute at all to the two-lepton sample.

In order to pass the charged track multiplicity cut in Table 4. 1, the tau pair events must satisfy one or more of the following requirements :

- One of the taus decays to more than four charged tracks.
- Both taus decay to three or more charged tracks.
- One of the taus decays to three (or more) charged tracks and there is an undetected Dalitz π^0 decay or photon conversion.

The probability that a tau decays to three charged tracks is ~ 20%, while the probability that it decays to five or more charged tracks is ~ 0.15%. The vast majority of all tau pair events will therefore fail our hadronic event selection cuts.

In order to be included in the one lepton sample both taus would have to decay to at least three charged tracks, and one of these hadrons would be have to be misidentified as, or decay to, a lepton. To be included in the two-lepton sample there would have to be an additional misidentified hadron or decay lepton.

In order to estimate the number of tau-pair events which pass our event selection cuts we used a tau-pair generator[27], combined with a full detector simulation, including the estimated hadronic misidentification probabilities, listed in Table 3. 2 and Table 3. 5 to generate a large sample of tau-pair events. From this sample we expect 439 ± 25 events to pass the hadronic event selection cuts, 42 ± 8 events to pass the single lepton cuts (of which ~ 95% were single electron events), and 2.6 ± 1.8 events to pass the dilepton cuts. These numbers represent 0.5% of the hadronic event sample, 0.5% of the single lepton sample, and 0.8% of the dilepton sample.

Backgrounds: *beam-gas events*

It is possible for a beam particle to interact with a proton or neutron in a gas molecule in the beam pipe, and for the resulting particles to be scattered into the detector In practice these events have a large amount of energy missing, and the probability of having *two* identified leptons present is negligible.

Chapter 5

Determining the dilepton composition

In this chapter we use the data to estimate the composition of the two-lepton sample. In order to demonstrate that the various components of the lepton samples are well understood, we account for the observed one- and two-lepton samples in terms of the possible sources of leptons. From a simultaneous fit to the one- and two-lepton samples we are able to extract the relative numbers of leptons from these sources, and estimate the composition of the two-lepton sample.

Because the kinematics of the semileptonic decays of B hadrons are independent of the charge of the lepton produced, it is not necessary to consider these charges, and therefore this procedure does not, to first order, affect the determination of the mixing parameter χ.

The fit procedure

The single lepton events allow a precise estimation of the relative amounts of leptons from different sources in the data. Because the fragmentation and decay of the two produced quarks in an event are assumed to take place independently, the results of a study of the one-lepton events are directly applicable to events in which both produced quarks decay to identified leptons.

The leptons present in the one- and two-lepton samples can be grouped into five distinct categories :

- Semileptonic decays of B hadrons — "B-primary" decays.
- Semileptonic decays of C hadrons in $c\bar{c}$ events — "C-primary" decays.
- Semileptonic decays of C hadrons in $b\bar{b}$ events — "B-secondary" decays.
- Misidentified hadrons — the "misid" component.
- Leptons from photon conversions and π, K decays — the "decay" component.

We used the Monte Carlo to produce a large, unbiased sample of leptons of all these types. As described in Chapter 3, the "misid" component was generated by using the hadronic misidentification probabilities, listed in Table 3. 2 and Table 3. 5. Each stable hadron which fell within the calorimeter or muon system acceptances was binned in momentum and transverse momentum†. Two random numbers between 0 and 1 were generated, and if the first was less than or equal to the per track electron misidentification probability for that p, p_t bin, the track was classified as a "misid" electron. If the second number was less than or equal to the per track muon misidentification probability for that bin, the track was classified as a "misid" muon. In the very small number of cases where the random numbers were *both* smaller than the misidentification probabilities, two new random numbers were generated.

To extract the relative amounts of these different lepton types present in the one- and two-lepton samples, we performed a binned maximum likelihood fit. For the one-lepton sample, we fit to the distribution of events binned in the two-dimensional p, p_t plane. For the two-lepton sample, we fit to the distribution of events binned in the two-dimensional *momentum cross product, minimum transverse momentum* plane. Both samples were fit simultaneously using the variables listed in Table 5. 1.

In order to check our *a priori* estimates of the misidentification and decay lepton

† As noted in Chapter 1, our definition of transverse momentum is the component of the track momentum perpendicular to the direction of the nearest reconstructed charged particle cluster.

Fit variables	
1)	electron misid scale
2)	electron decay scale
3)	$Br(B \rightarrow e)$
4)	$Br(C \rightarrow e)$
5)	muon misid scale
6)	muon decay scale
7)	$Br(B \rightarrow \mu)$
8)	$Br(C \rightarrow \mu)$

Table 5. 1

distributions, we included a scale factor for each of the four separate distributions (electron misid, electron decay, muon misid and muon decay). These scale factors (which have no p or p_t dependence) would have the value 1.0 if our original estimates had been exactly correct.

The total numbers of produced $c\bar{c}$ and $b\bar{b}$ events were predicted from the Monte Carlo. However, within these events, we allowed the probability that the produced quarks decayed to leptons to vary. These semileptonic branching ratios have been measured by several experiments, and the values we extracted from the fit were an important cross-check on the analysis procedure.

The one-lepton sample

The predicted number of leptons of type l (either electron or muon) in a given p, p_t bin in the one-lepton sample is given by :

$$\begin{aligned} PRED_l(p, p_t) = \; & Bpri(p, p_t) \cdot \frac{\varepsilon_{data} \cdot Br(B \rightarrow l)}{\varepsilon_{mc} \cdot Br(B \rightarrow l)_{mc}} \\ & + Bsec(p, p_t) \cdot \frac{\varepsilon_{data} \cdot Br(C \rightarrow l)}{\varepsilon_{mc} \cdot Br(C \rightarrow l)_{mc}} \\ & + Cpri(p, p_t) \cdot \frac{\varepsilon_{data} \cdot Br(C \rightarrow l)}{\varepsilon_{mc} \cdot Br(C \rightarrow l)_{mc}} \\ & + Misid(p, p_t) \cdot misid\ scale\ factor \\ & + Decay(p, p_t) \cdot decay\ scale\ factor \end{aligned}$$

Where $PRED_l(p, p_t)$ is the total predicted number of leptons of type l in one-lepton events in the given (p, p_t) bin; *Bpri*, *Cpri*, *Bsec*, *Misid* and *Decay* (p, p_t) are the pre-

dicted numbers of B-primary, C-primary, B-secondary, "misid" and "decay" leptons of type l in the given (p, p_t) bin; $Br(B \rightarrow l)$, $Br(C \rightarrow l)$, *misid scale factor* and *decay scale factor* are the variables used in the fit; $Br(B \rightarrow l)_{mc}$ and $Br(C \rightarrow l)_{mc}$ are the semileptonic branching ratios in the Monte Carlo, and ε_{mc} and ε_{data} are the lepton identification efficiencies in the Monte Carlo and the data, respectively. These efficiencies are listed in Table 3. 1 and Table 3. 4.

The bins were 0.5 GeV/c wide in both momentum and transverse momentum. Recalling the cuts applied to the single-lepton sample, listed in Table 4. 2, the bins ranged from 1.0–9.0 GeV/c and 0.0–3.5 GeV/c for the electron momentum and transverse momentum, respectively, and from 1.5–9.0 GeV/c and 0.0–3.5 GeV/c for the muon momentum and transverse momentum.

The log likelihood of observing $DATA_l(p, p_t)$ leptons, given the predicted number $PRED_l(p, p_t)$, was then formed using Poisson statistics, and this likelihood was summed over all (p, p_t) bins to form the overall log likelihood, $L_{one\text{-}lepton}$ (a function of the eight fit variables) :

$$L_{one\text{-}lepton} = L_e + L_\mu$$

$$\text{where :} \quad L_l = -\left\{ \sum_{all\ bins} \log\left[\frac{x^n \exp(-x)}{n!}\right] \right\}$$

$$x = PRED_l(p, p_t)$$

$$n = DATA_l(p, p_t)$$

$$l = e, \mu$$

The two-lepton sample

Because of the relatively large numbers of one-lepton events, the fit parameters were much more sensitive to the one-lepton sample than to the two-lepton sample. However, the two-lepton sample was used to extract the mixing information, and therefore it is important that the predicted dilepton distributions in the *momentum cross product vs. minimum transverse momentum* plane agree with the observed distributions.

Obtaining the predicted two-lepton distributions was more complicated than the one-lepton distributions. In principle, one could have generated very large numbers of Monte Carlo events (perhaps 25 times the size of the total hadronic data sample), and used the two-lepton distributions obtained from this large sample. In practice, this approach was not feasible because of the huge amount of computing time that would be required to generate so many events.

We chose to use the Monte Carlo to selectively generate large numbers of each of the possible two-lepton types, thereby obtaining the *shape* of each distribution, while using the fit variables to predict the absolute *normalization* for each distribution. We describe these two separate steps in the following sections.

Obtaining the *shapes* of the two-lepton distributions

There is a large number of possible combinations of dilepton types in the data. These possible combinations are listed in Table 5. 2. For each dilepton type listed there are three distinct *classes* of dilepton, namely electron-electron, electron-muon and muon-muon events. In order to generate the necessary number of events of each dilepton type (which were typically 5-25 times the number expected in the data) we selectively generated large numbers of $b\bar{b}$ and $c\bar{c}$ events with values of the semileptonic branching ratios twice their standard values.

We also obtained large samples of "misid" leptons by increasing the per track misidentification probabilities by a factor of five. The only events which did not have more than five times the expected number in the data were those involving "decay" leptons. This was because we had no straightforward, unbiased way of increasing the "decay" probabilities. Fortunately, the expected number of dileptons involving decay leptons was relatively small, and these did not form a serious background to the region containing the signal.

The bins in the *momentum cross product vs. minimum transverse momentum* plane had dimensions 1.5 $(\text{GeV/c})^2$ by 0.5 GeV/c, respectively, and entries with $mcp > 15$ $(\text{GeV/c})^2$

or *min* p_t > 3.5 GeV/c were included in the edge bins†. There was a total of 70 bins in the entire plane.

Possible dilepton types

event flavor					
$b\bar{b}$	Bpri-Bpri,	Bpri-Bsec,	Bsec-Bsec,	Bpri-misid,	Bsec-misid,
	misid-misid,	misid-decay,	decay-decay,	Bpri-decay,	Bsec-decay.
$c\bar{c}$	Cpri-Cpri,	Cpri-misid,	Cpri-decay,		
	misid-misid,	misid-decay,	decay-decay.		
$u\bar{u}$, $d\bar{d}$, $s\bar{s}$	misid-misid,	misid-decay,	decay-decay.		

Table 5. 2

Obtaining the *normalization* of the two-lepton distributions

In order to obtain the normalization for each of the possible two-lepton final states, based on the variables used in the fit, it was necessary to assume that the two produced quarks in an event hadronized and decayed independently of each other. Given this assumption, it was possible to use the one-lepton data sample to estimate the probability that a given type of produced quark (*e.g.*, a charm quark) decayed to a particular type of identified lepton (*e.g.*, a "misid" electron). The probability that *both* produced charm quarks in an event decayed to give "misid" electrons was then simply the square of the one-lepton probability. Using this method it was possible to estimate the probabilities for all possible two-lepton final states from an event of a given flavor.

The estimation of the normalization for each of the possible two-lepton final states consisted of the following steps (an example of this estimation is given in Appendix B) :

† For brevity we refer to *momentum cross product* as *mcp*, and to *minimum transverse momentum* as *min* p_t.

i) The Monte Carlo was used to estimate the total number of events of each quark flavor in the hadronic data sample.

ii) The total number of leptons of a given type in the one-lepton sample (*e.g.*, B-primary muon) was obtained from the fit parameters and the predicted one-lepton distribution for that lepton type.

iii) The probability that a given quark flavor decayed to the given lepton type was then the total number of the given lepton type in the one-lepton sample divided by the total number of produced quarks of the given flavor (assumed to be twice the number of events of that flavor) in the hadronic data sample. For the misid and decay leptons, which could have been produced by events of any flavor, the expected number of leptons of the given type *produced in events of the given flavor* was divided by the number of events of that flavor to yield the required probability.

iv) The probability that *both* quarks in a given event decayed to identified leptons was then calculated by multiplying the number of events of the given flavor in the hadronic data sample by the two single-lepton probabilities, calculated in *iii)*. The total number of two-lepton events of the given type was then simply the total number of events of that flavor in the hadronic data sample multiplied by the probability that both quarks decayed to the required leptons.

v) This number of two-lepton events of the given type needed to be corrected for the following effects :

- *Differences in the event selection cuts for the one- and two-lepton data samples.* Since the one-lepton cuts were stricter than the two-lepton cuts, the Monte Carlo was used to estimate the efficiency for both leptons in a two-lepton event to pass the one-lepton event cuts (had we neglected this effect we would have underestimated the number of two-lepton events of the given type in the two-lepton sample). This efficiency was ~ 88% for B-primary leptons and ~ 95-99% for other lepton types. We divided by this efficiency to estimate the total number of events which would have passed the two-lepton event cuts.

- *Correlations in the detector acceptance.* Since the Muon System, shown in Figure 2. 1, is not azimuthally symmetric, the probability of detecting two muons in opposite jets is not simply the square of the probability of detecting a single muon. Because of the two-jet structure of the majority of events, when one muon has been detected, the opposite jet is likely to be pointing into the Muon System, and therefore the probability of detecting a second muon is higher than for an event which was randomly oriented in phi. This effect increases the dimuon identification efficiency by ~ 37%. The LA Calorimeter is effectively azimuthally symmetric, and therefore the dielectron and electron-muon identification efficiencies were not affected by acceptance correlations.

We show four of the predicted dielectron distributions in Figure 5. 1.

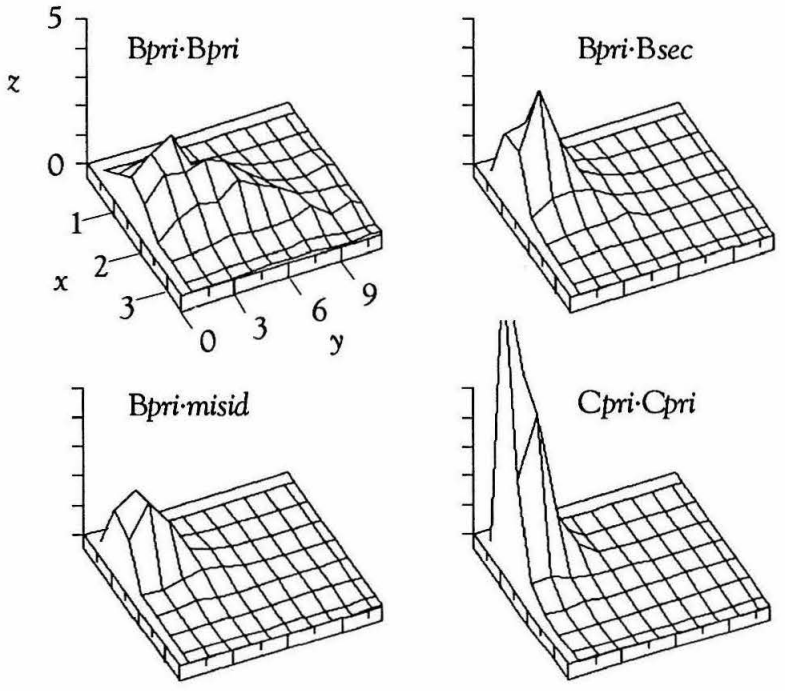

x = *minimum pt* (GeV/c)

y = *momentum cross product* $(\text{GeV/c})^2$

z = *dileptons* $/(\ 0.5\ \text{GeV/c}) \times (\ 1.5\ (\text{GeV/c})^2)$

Figure 5. 1

Because the one-lepton probabilities calculated in step *ii)* depended on the fit parameters, the normalization for each dilepton type was also a function of these parameters (clearly if, say, the muon misid scale factor increased, then the expected numbers of dileptons involving misid muons would also increase). Given the *shapes* and the *normalizations* of the dilepton distributions we were able to predict the absolute number of dileptons of each type in each bin in the *mcp*, *min* p_t plane, as a function of the eight fit variables. We call this predicted number of dileptons of a given type $pred_{ll}$ (*i*, *j*, *mcp*, *min* p_t), where *l* can be electron or muon; *i* and *j* can be *Bpri*, *Bsec*, *Cpri*, *misid* or *decay*; and *mcp* and *min* p_t are the momentum cross product and the minimum transverse momentum, respectively. We sum these numbers over the *i* and *j* indices to obtain $PRED_{ll}$ (*mcp*, *min* p_t), the total predicted number of dileptons in a given bin for the three observable classes *ee*, *eμ* and *μμ*.

The log likelihood of then observing $DATA_{ll}$ (*mcp*, *min* p_t) dileptons given the predicted number $PRED_{ll}$ (*mcp*, *min* p_t) was then formed using Poisson statistics, and this likelihood was summed over all *mcp*, *min* p_t bins to obtain the three likelihoods L_{ee}, $L_{\mu\mu}$ and $L_{e\mu}$, and finally the overall two-lepton likelihood, $L_{two\text{-}lepton}$ (a function of the eight fit variables) :

$$L_{two\text{-}lepton} = L_{ee} + L_{e\mu} + L_{\mu\mu}$$

$$\text{Where :-} \quad L_{ij} = -\left\{ \sum_{all\ bins} log\left[\frac{(x_{ij})^{n_{ij}} exp(-x_{ij})}{n_{ij}!} \right] \right\}$$

$$n_{ij} = DATA_{ij}\ (mcp, min\ p_t)$$

$$x_{ij} = PRED_{ij}\ (mcp, min\ p_t)$$

$$PRED_{ij}\ (mcp, min\ p_t) = \sum_{k,l} pred_{ij}(k, l, mcp, min\ p_t)$$

$$i, j = electron, muon$$

$$k, l = Bpri, Bsec, Cpri, misid, decay$$

To obtain the final likelihood we added together the one- and two-lepton likelihoods :

$$L_{overall} = L_{one\text{-}lepton} + L_{two\text{-}lepton}$$

This function was then maximized by varying the eight fit parameters. The most likely values of these parameters, listed in Table 5. 3, were those which maximized $L_{overall}$.

Results of the fit

The results of the fit are summarized in Table 5. 3. There are three important points to be made :

- The semileptonic branching ratios are in good agreement with the current World Average values[28]. (These World Averages do not include previous Mark II analyses.) They are also in agreement with the previous Mark II inclusive lepton analyses[16,22].
- The electron and muon *a priori* background estimates are consistent with the data. This can be seen from the fact that the e background and μ background variables (described below) were consistent with the value 1.0, within the expected errors.
- The predicted numbers of dilepton events agree well with those observed.

The systematic errors listed in Table 5. 3 are discussed in Chapter 7.

To check the overall consistency of the results, we also performed fits where we maximized the quantities $L_{one\text{-}lepton}$ and $L_{two\text{-}lepton}$ separately. These are referred to in Table 5. 3 as the one-lepton fit and the two-lepton fit, respectively. The errors listed for the one- and two-lepton fits are the one standard-deviation statistical errors derived from the likelihood function (*i.e.*, the variation in the given parameter which decreased the log likelihood by 0.5 units from its maximum value). The two errors listed for the combined fit are the statistical and systematic errors, respectively. Although we did not use the semileptonic branching ratios listed in Table 5. 3 elsewhere in this thesis, they served as a useful cross-check on the estimation of the composition of the dilepton sample.

Results of inclusive lepton fits

parameters	*one-lepton fit*	*two-lepton fit*	***combined fit***	*World Average*
Br (B $\rightarrow e$) %	15.5 ± 1.0	11.3 ± 1.7	$\mathbf{13.7 \pm 0.8 \pm 1.3}$	12.5 ± 1.3
Br (B $\rightarrow \mu$) %	15.5 ± 1.3	8.8 ± 3.5	$\mathbf{13.7 \pm 1.1 \pm 1.1}$	12.4 ± 1.0
Br (C $\rightarrow e$) %	10.1 ± 0.8	9.8 ± 3.1	$\mathbf{11.0 \pm 0.8 \pm 1.7}$	10.2 ± 0.8
Br (C $\rightarrow \mu$) %	7.0 ± 1.2	11.3 ± 3.3	$\mathbf{7.9 \pm 1.1 \pm 1.2}$	8.2 ± 0.8
				stat $\oplus$ *sys*
e background	1.04 ± 0.06	1.19 ± 0.25	$\mathbf{1.03 \pm 0.05 \pm 0.40}$	
μ background	0.87 ± 0.05	0.69 ± 0.20	$\mathbf{0.86 \pm 0.04 \pm 0.35}$	
	stat.	*stat.*	*stat.* *sys.*	

dilepton class	*one-lepton fit*	*two-lepton fit*	***combined fit***	*observed*
electron-electron	199.4	182.9	**194.3**	191
electron-muon	117.5	112.7	**114.8**	117
muon-muon	25.2	23.9	**24.5**	23

Table 5. 3

Although we used the log likelihood variable to extract the most likely values of the fit parameters, to obtain a quantitative estimate of the quality of the fit we calculated the chi-square quantity defined by:

$$\chi^2_{e,\mu} = \sum_{\textit{all bins}} \frac{[\,\text{observed}(p, p_t) - \text{predicted}\,(p, p_t)\,]^2}{\text{predicted}\,(p, p_t)}$$

This quantity was only calculated for the one-lepton sample because the Gaussian approximation used was not appropriate for the small numbers of events in many of the bins of the two-lepton sample. The calculated chi-square was 119 for 94 degrees of freedom for the one-electron sample†, and 88 for 91 degrees of freedom for the one-muon sample.

† One bin in which approximately five events were predicted and none was observed contributed 24.1 to the total chi-square for the one-electron sample. This bin appeared to be a statistical fluctuation.

The rows labeled "*e* background" and "μ background" in Table 5. 3 deserve further comment. These are the combined values for the misid and decay scale factors for electron and muons, respectively. Because the misid and decay components tended to occupy the same regions of the p, p_t plane in the one-lepton sample, the scale factors for these components were very highly anti-correlated in the fit. Because of this anti-correlation, the only quantity which made physical sense in the context of the fit was the *sum* of the two components. The quantities *e* background and μ background were therefore defined by :

$$e, \mu \text{ background} = \frac{\sum_{\text{all bins}} (misid + decay)_{fit}}{\sum_{\text{all bins}} (misid + decay)_{a\ priori}}$$

Although we have lost some information in defining this quantity (namely the relative quantities of misid and decay), this information is not accessible in the fit. The fact that the *a priori* estimates for the electron and muon decay and misid backgrounds agreed with the amount observed in the data, within the estimated systematic errors of the background determination, gives confidence that these backgrounds are understood.

The predictions for the total number of dileptons of each class, based on the fit parameters, are also given in Table 5. 3. While one would expect the two-lepton data to strongly influence the total number of two-lepton events predicted, the fact that predictions from the statistically independent one-lepton fit also give good agreement with the observed number of two-lepton events gives confidence in the overall procedure. In Figure 5. 2 through Figure 5. 11 we show the predicted and observed one- and two-lepton distributions.

Up to this point we have made no assumptions about the charges of the leptons. In fact, all the inclusive lepton fit results are independent of the extent of mixing: a lepton from a B^0 primary decay is kinematically equivalent to one from a $\overline{B}^0$ primary decay.

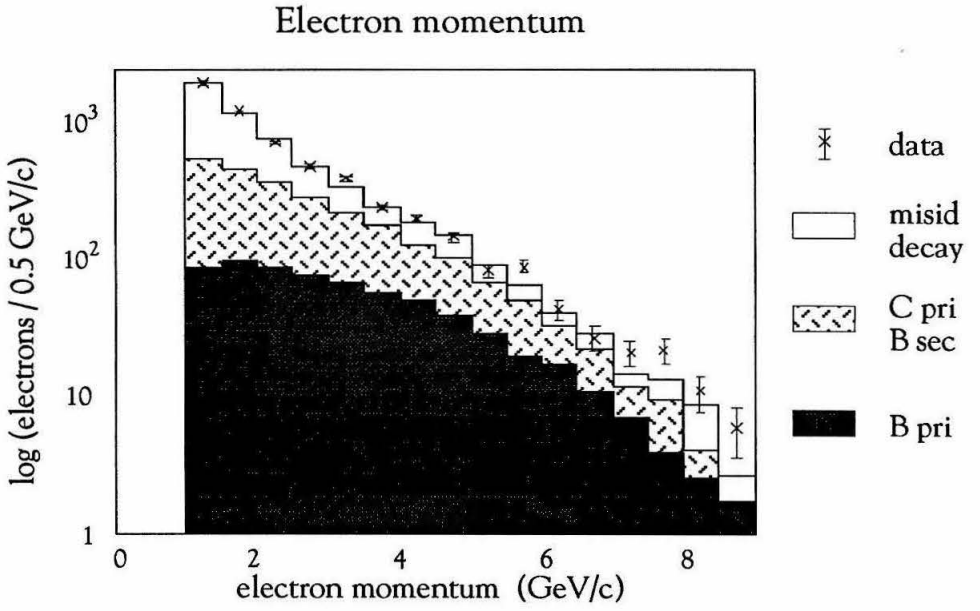

Figure 5. 2

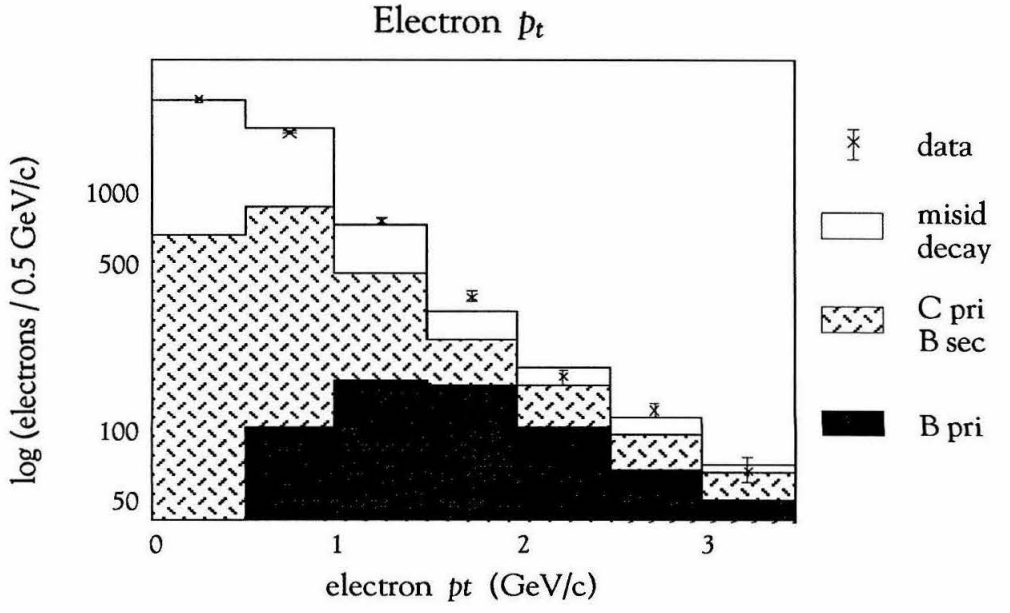

Figure 5. 3

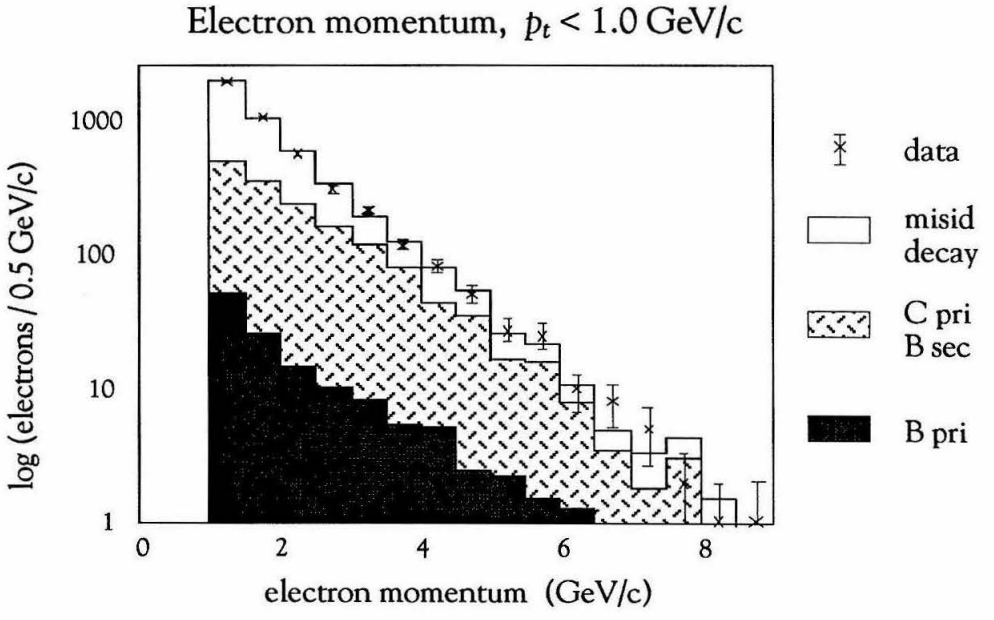

Figure 5. 4

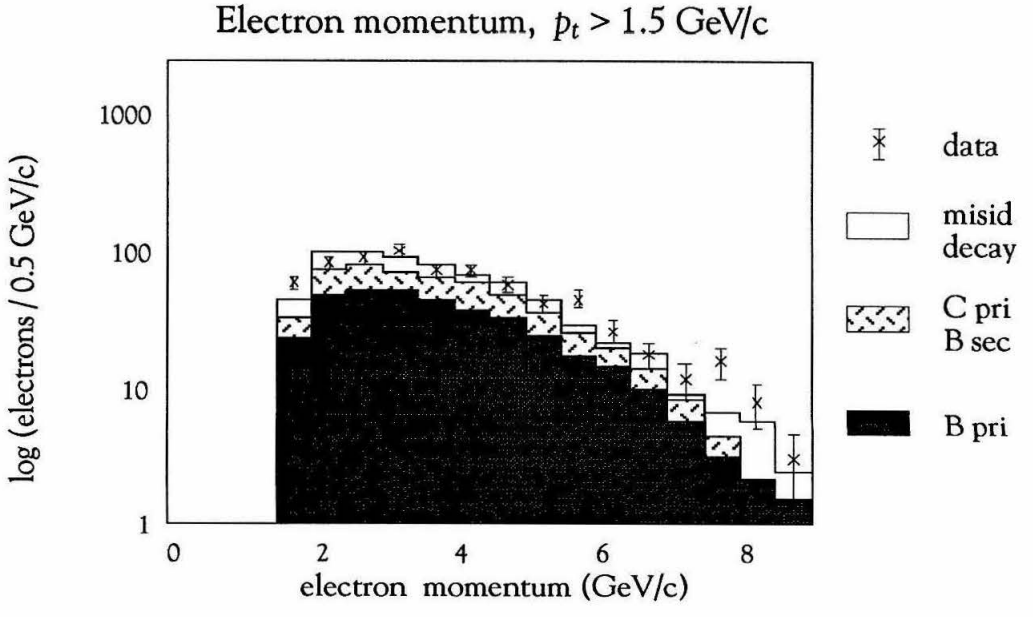

Figure 5. 5

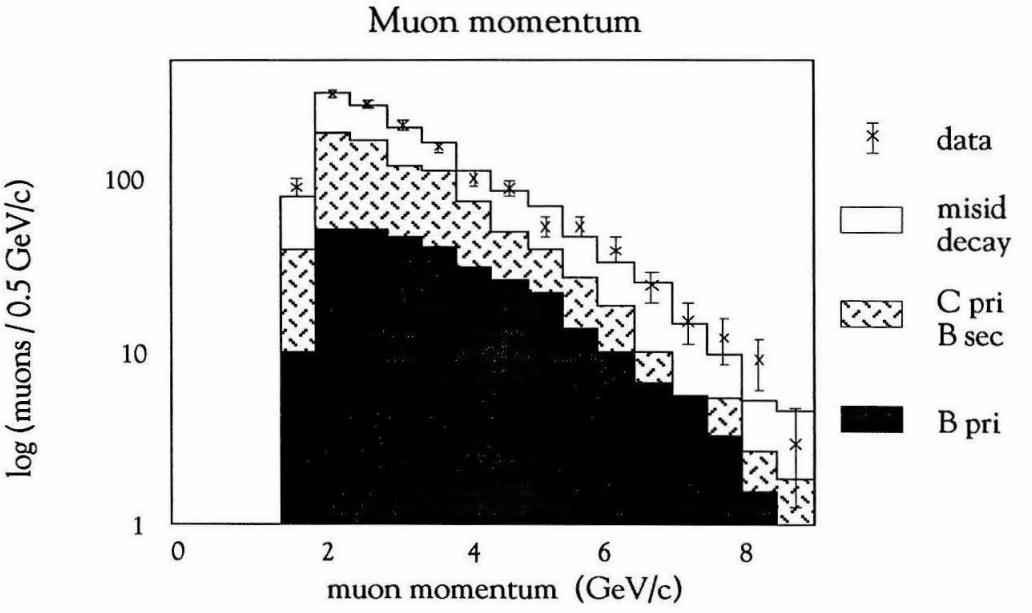

Figure 5. 6

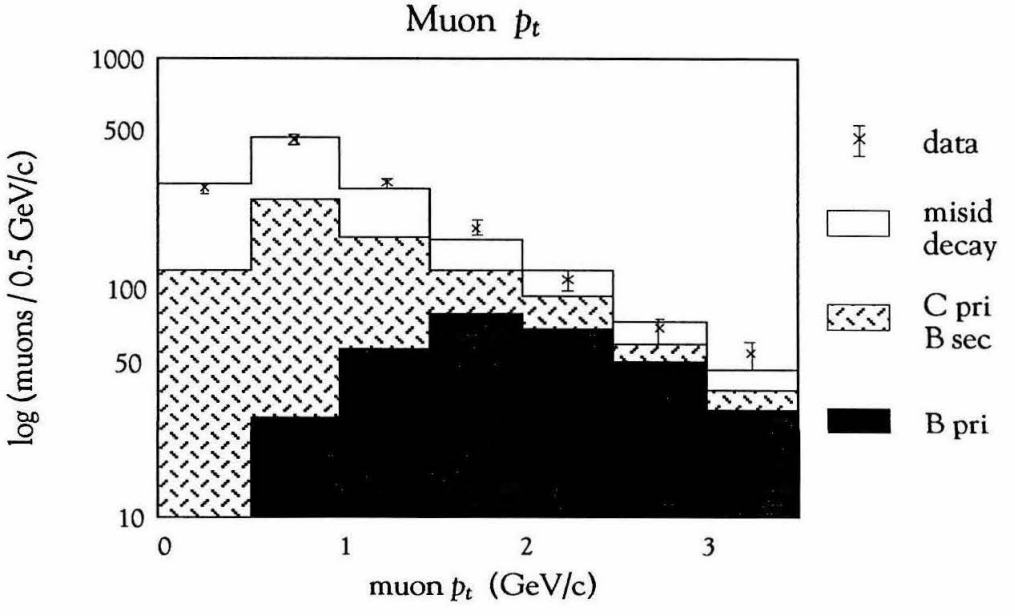

Figure 5. 7

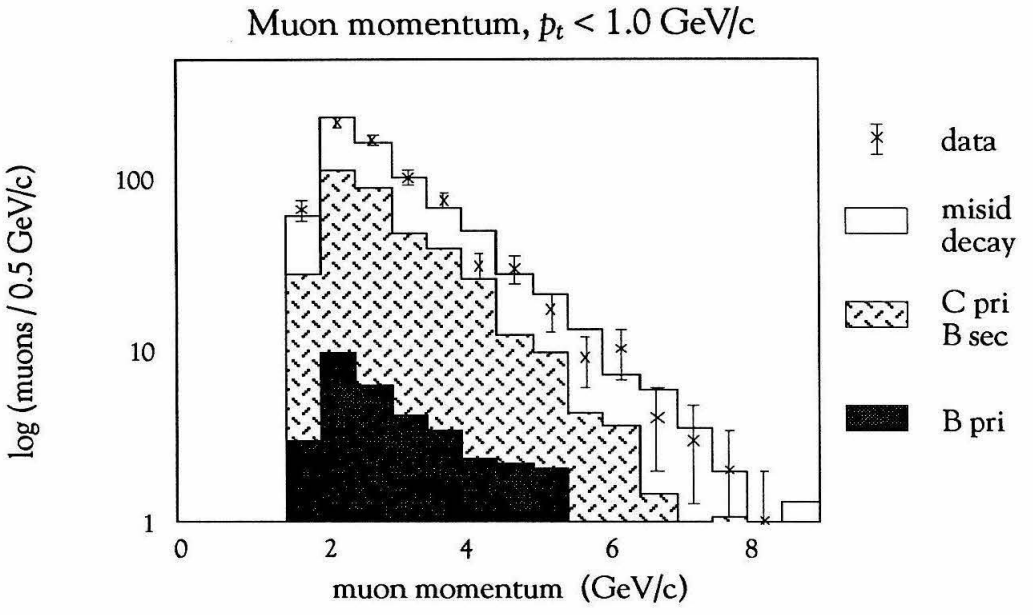

Figure 5. 8

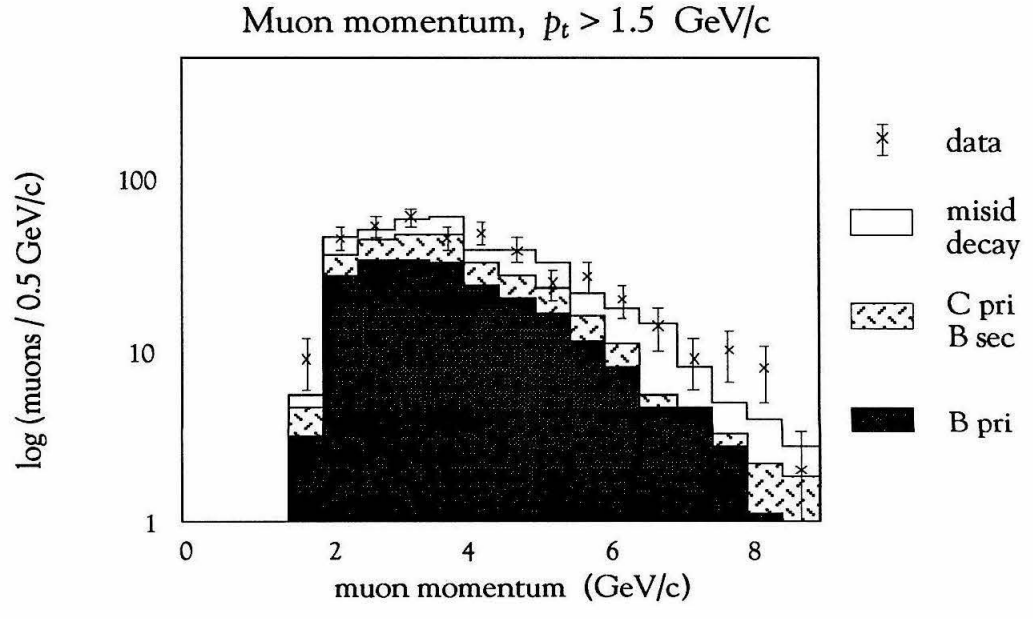

Figure 5. 9

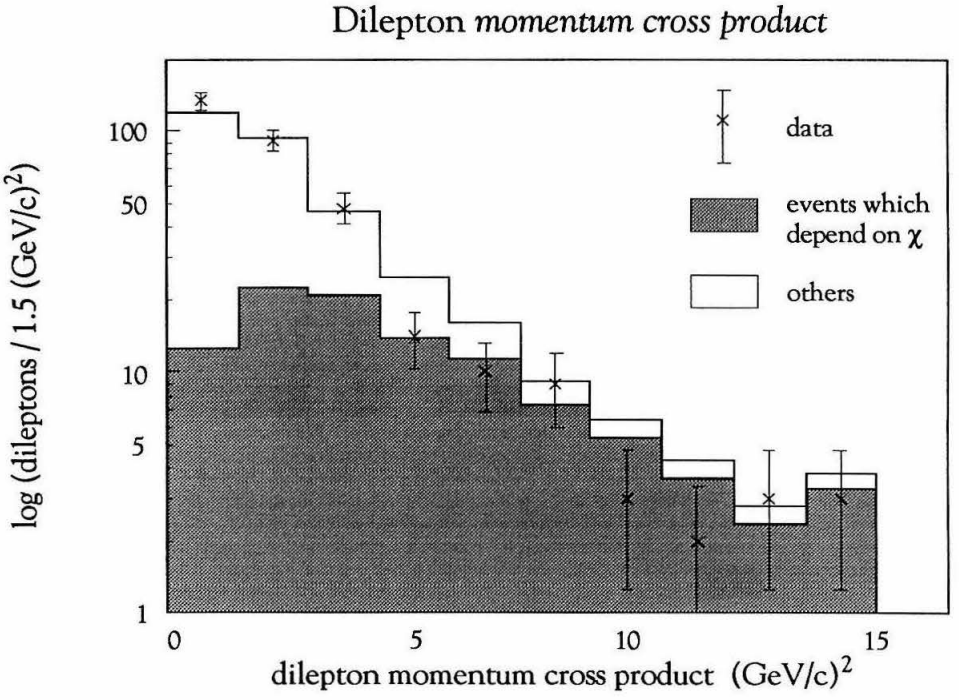

Figure 5. 10

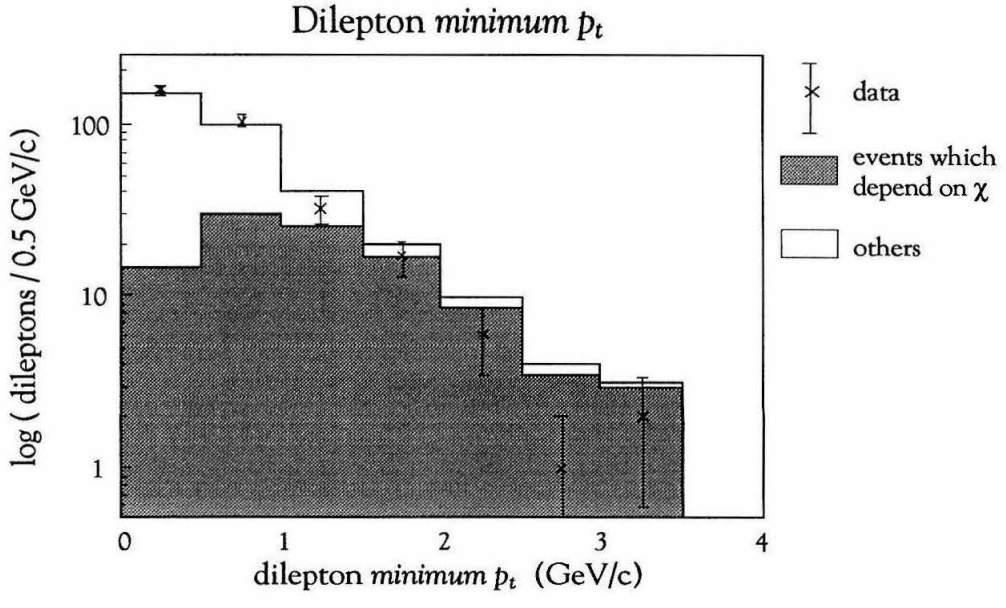

Figure 5. 11

Chapter 6

The mixing likelihood function

GIVEN the composition of the two-lepton sample, as determined by the fit described in Chapter 5, it is possible to predict the relative numbers of like-sign and unlike-sign dileptons *in each bin* of the *momentum cross product vs. minimum* p_t plane. To make these predictions, we assume the following :

i) Any two-lepton event which contains one or two *misid* or *decay* leptons has equal probabilities for the leptons to have the same or opposite signs.

ii) All two-lepton events in which both leptons come from C-primary decays have opposite signs†.

iii) The fraction of B-secondary-B-secondary two-lepton events which have the same sign is given by $2\chi\,(1-\chi)$.

iv) The fraction of B-primary-B-secondary two-lepton events which have the same sign is given by $1-2\chi\,(1-\chi)$.

v) The fraction of B-primary-B-primary events which have the same sign is given by $2\chi\,(1-\chi)$.

Where, as we recall from Chapter 1, χ is defined as the fraction of all B-primary decays which result in a lepton of the "wrong" sign.

† We assume that D-mixing is negligible.

In practice, several of these assumptions need to be modified slightly to account for the following effects :

- *Quark charge retention in jets.* In events where a charged hadron is produced with a large fraction of the parent quark charge, the charge of the hadron can be correlated with the charge of the quark[29]. To estimate the size of this effect, the single-lepton data sample was used, along with a large sample of single-lepton Monte Carlo events. All charged tracks which fell within the Calorimeter and Muon System acceptances, and were separated by more than 90° from the lepton, were paired with the lepton to check for possible charge correlations. The ratio of the number of opposite-sign pairs to same-sign pairs was determined from both the data and the Monte Carlo to be 1.066 ± 0.028. The Monte Carlo did not reveal any statistically significant dependence on the quark flavor of the event. Also, events in which the dilepton momentum cross product was more than 10 $(\text{GeV/c})^2$ did not show an appreciably larger charge correlation than other events. This effect was included for all two-lepton events involving a *misid* or *decay* lepton.

- *B-secondary decays.* We have assumed that the sign of a "B-secondary" lepton in an unmixed b quark jet is always positive, while the sign of a "B-primary" lepton from a b quark decay is always negative. In fact, it is possible (although unusual) for more than one charmed hadron to be produced in the hadronization of a b or $\overline{b}$ quark. If the B-secondary lepton comes from such a charmed hadron, its charge is not necessarily correlated with the original b or $\overline{b}$ quark charge. This effect was studied by using two separate Monte Carlo hadronization models — the Lund parton shower model[30] with Lund symmetric fragmentation, and the Lund 2nd order matrix element model[31] with Peterson fragmentation. Both models were consistent in predicting that, in the absence of mixing, $14 \pm 2\%$ of B-primary-B-secondary two-lepton events have the *opposite* sign. This effect was included for all B-primary-B-secondary events. We also estimated that $20 \pm 4\%$ of unmixed B-secondary-B-secondary events have the *same* sign, and included this effect for all B-secondary-B-secondary events.

Using these assumptions, and the correctly normalized *momentum cross product vs.*

minimum pt distributions, we obtained predictions for the expected number of like- and unlike-sign dileptons for each bin in the distribution, as a function of the mixing parameter, χ. The log likelihood was then calculated for the observed number of like- and unlike-sign dileptons of a given class (*i.e.*, electron-electron, electron-muon or muon-muon) in each bin and the total log likelihood for that class, $L_i(\chi)$, was formed by adding the log likelihoods for all bins together. The overall log likelihood function, $L(\chi)$, was then the sum of the three $L_i(\chi)$s.

$$L_i(\chi) = -\left\{ \sum_{\text{all bins}}^{\text{same sign}} \log\left[\frac{x_i^{n_i}\, exp(-x_i)}{n_i!}\right] + \sum_{\text{all bins}}^{\text{opp. sign}} \log\left[\frac{x_i^{n_i}\, exp(-x_i)}{n_i!}\right] \right\}$$

$$L(\chi) = \sum_{i = ee,\, e\mu,\, \mu\mu} L_i(\chi)$$

Where : n_i = number of observed dileptons of class i in a given bin

x_i = predicted total number of dileptons of class i in a given bin (a function of χ)

It is important that each class of dilepton has its own likelihood function. The previous Mark II B-mixing analysis treated the three classes as equivalent, generic dileptons. Unfortunately, this was incorrect because the relative normalizations and backgrounds are different. For example, the observation of a same-sign dimuon event is much more significant in terms of mixing than is a same-sign dielectron event, simply because there are many fewer dimuons than dielectrons, and the muon backgrounds are significantly smaller than the electron backgrounds.

A plot of the overall log likelihood function for χ is shown in Figure 6. 1. The dashed lines indicate the 1 sigma and 90% confidence level limits at which the log likelihood function is 0.5 and 0.83 units below the most likely value, respectively. The most likely value for χ is seen to be 0.17, with 90% confidence level upper and lower limits of 0.29 and 0.08, respectively. Also shown in Figure 6. 1 is the log likelihood function for the PEP5 data sample alone, which accounts for ~ 90% of the two-lepton events.

The log likelihood function for the mixing parameter, χ.

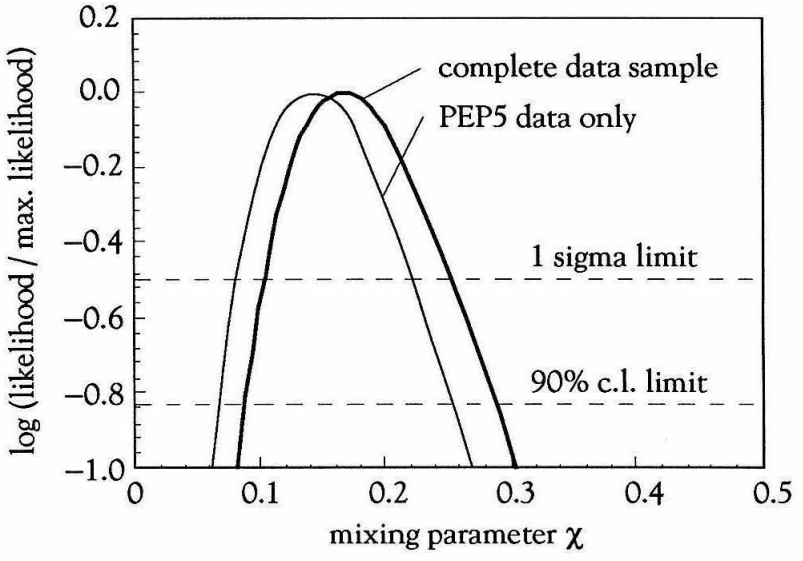

Figure 6. 1

The most likely value for χ is strongly determined by the relatively small number of events in the region with high values of the momentum cross product and minimum p_t variables. This is where there is the largest separation between the "signal" (B-primary-B-primary) and "background" (all others).

Table 6. 1 shows the observed and calculated numbers of events in restricted regions of the *momentum cross product vs. minimum* p_t plane. The numbers in parentheses are the predicted values for χ = 0, the numbers in brackets are the predicted values for χ = 0.17. There is clear evidence of an excess of same-sign events in the electron-muon and muon-muon classes, while the electron-electron class is consistent with zero mixing. The shape of the likelihood function in Figure 6. 1 for values of χ less than about 0.10 is determined by the excess of like-sign events containing muons; for values of χ more than about 0.20 the shape is determined by the relative lack of like-sign electron-electron events. The difference between the likelihood functions in Figure 6. 1 is almost all due to the same-sign dimuon event in Table 6. 1 which occurred in the Upgrade running.

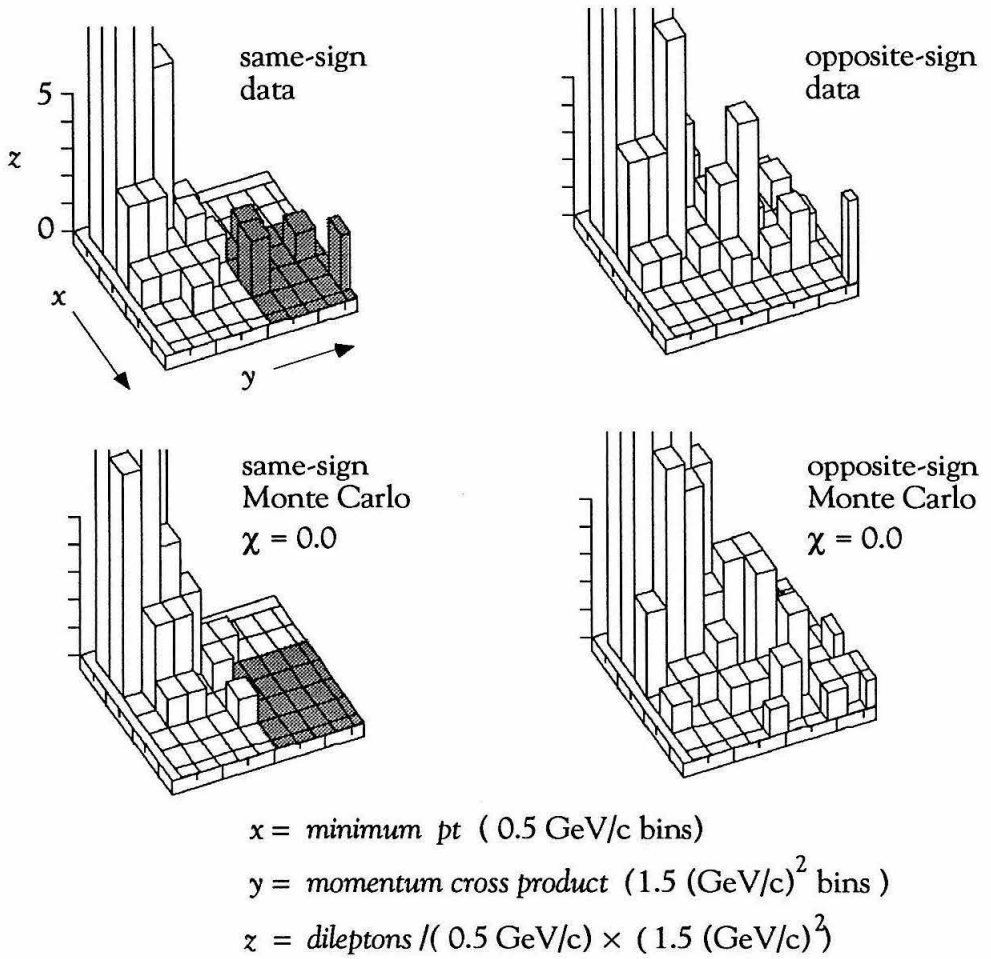

Figure 6. 2.

Figure 6. 2 shows the expected numbers of same-sign and opposite-sign events in the *momentum cross product vs. minimum* p_t plane for the data and a sample of Monte Carlo events with zero mixing†. The region with $mcp > 7.5$ (GeV/c)^2 and *minimum* $p_t > 1.0$ GeV/c is indicated by shading. There is a clear excess of same-sign events in this shaded region when compared to the Monte Carlo.

† The predictions in Table 6. 1 were obtained from the fit results in Chapter 5. The events in Figure 6. 2 were from a single sample of Monte Carlo events with zero mixing to show typical statistical fluctuations.

Results for the region most sensitive to mixing

mom. cross product > 7.5 $(GeV/c)^2$,
min. p_t > 1.0 GeV/c

	opposite sign			*same sign*			*both signs*	
e-e	9	(8.0)	[6.3]	2	(1.4)	[3.1]	11	(9.3)
e-μ	5	(9.4)	[7.4]	3	(1.7)	[3.8]	8	(11.1)
μ-μ	1	(2.7)	[2.1]	1	(0.4)	[1.0]	2	(3.1)
total	15	(20.1)	[15.8]	6	(3.5)	[7.9]	21	(23.5)

mom. cross product > 12.0 $(GeV/c)^2$,
min. p_t > 1.5 GeV/c

	opposite sign			*same sign*			*both signs*	
e-e	2	(1.3)	[1.1]	0	(0.33)	[0.56]	2	(1.7)
e-μ	2	(2.4)	[1.8]	2	(0.23)	[0.82]	4	(2.7)
μ-μ	0	(0.61)	[0.44]	1	(0.02)	[0.19]	1	(0.63)
total	4	(4.3)	[3.3]	3	(0.58)	[1.57]	7	(5.0)

numbers in parentheses are the predictions with $\chi = 0$
numbers in brackets are the predictions with $\chi = 0.17$

Table 6. 1

In Chapter 7 we investigate the possible sources of systematic error on this measurement of the mixing parameter, χ.

Chapter 7

Systematic errors

We now investigate the possible sources of systematic error which affect the value of χ measured in Chapter 6. These sources of error can be logically grouped into four categories :

- Uncertainties in the Monte Carlo event generation and background estimation.
- Biases introduced by the procedure used to measure χ .
- Errors in the assumptions about charge correlations between the dileptons.
- Detector effects.

We begin by discussing the errors associated with the Monte Carlo.

Errors associated with the Monte Carlo

• *The bottom and charm fragmentation functions.* Because our understanding of the fragmentation process is only phenomenological, there is uncertainty associated with the particular form chosen for the parametrization of the fragmentation observables. Previous analyses[4] have shown that fits to the data depend more on the mean value of the fragmentation function than on the detailed shape of the function itself. A previous Mark II analysis involving inclusive leptons[3] has set limits on the allowed variation of the mean value, $\langle z_b \rangle$, of the bottom quark fragmentation function, which translate into

upper and lower limits on the Peterson function ε_b value. This allowed range of values of the mean of the bottom quark fragmentation function was determined to be $\langle z_b \rangle = 0.85 \pm 0.06$ for electrons, and $\langle z_b \rangle = 0.82 \pm 0.07$ for muons, which translate into variations in ε_b given by $\varepsilon_b = 0.005^{+0.005}_{-0.004}$.

The allowed variation in the mean of the charm fragmentation function was $\langle z_c \rangle = 0.68 \pm 0.06$, the same as that assumed in the previous inclusive lepton analysis. This variation allowed for the finite precision of the D^* fragmentation measurements and the use of parametrizations other than the Peterson fragmentation function.

To check that the assumed values for the fragmentation function parameters were indeed optimal, the fit, described in Chapter 5, was repeated using the possible combinations of the extreme values of the bottom and charm fragmentation parameters. In all cases, the fit was worse (*i.e.*, the likelihood was smaller) when the extreme values were chosen.

Because of the good separation of B-primary-B-primary dileptons from those containing leptons from charm decays, variations in the charm fragmentation function made a negligible difference to the mixing likelihood function. In principle, variations in the bottom quark fragmentation parameters could have had an important effect on the mixing result, since the predicted momentum spectrum of the B-primary leptons is strongly affected by such variations. However, in practice, the small allowed variations in the bottom fragmentation function led to a relatively modest change in the B-primary momentum spectrum. When ε_b was chosen to be 0.010 (soft fragmentation) the measured value for χ was $\chi = 0.18^{+0.14}_{-0.06}$, while for $\varepsilon_b = 0.001$ (hard fragmentation) the measured value was $\chi = 0.16^{+0.12}_{-0.06}$.

• *Lepton identification efficiencies.* The electron and muon identification efficiencies are listed in Table 3. 1 and Table 3. 4. The relevant parameter is the ratio of the identification efficiencies for the data and the Monte Carlo. We assumed a 5% error on this ratio. This error has essentially no effect on the mixing measurement because χ is only sensitive to the *relative* amounts of like-sign and unlike-sign dileptons and not to the absolute numbers of each.

• *The numbers of $b\bar{b}$ and $c\bar{c}$ events.* In calculating the probabilities for quarks of a given flavor to decay to identified leptons we used the Monte Carlo to estimate the numbers of events of each flavor in the hadronic event sample. To allow for differences in the acceptance for bottom and charm events due to uncertainties in the multiplicities and fragmentation schemes, we assigned a 5% error on the absolute number of bottom and charm events in the hadronic event sample. In effect, because the number of identified leptons is fixed, such variations are equivalent to variations in the semileptonic branching ratios for B and C decays. These variations also have very little effect on the mixing measurement because they affect like- and unlike-sign events equivalently through an overall normalization factor.

• *The semileptonic branching ratios for B, C $\rightarrow$ leptons.* In order to check the sensitivity of the mixing likelihood function to variations in the B and C semileptonic branching ratios , the values of these branching ratios were fixed at the World Average values, listed in Table 5. 3. There was effectively no change in the mixing likelihood function because these branching ratios merely affect the overall normalization of the B-primary, B-secondary and C-primary distributions.

• *Leptons from decays of tau leptons.* Although tau leptons have not been experimentally observed in multi-hadronic events at PEP or PETRA, it is believed that B hadrons can decay semileptonically to taus with a branching ratio of order 5%. In such cases, the tau can subsequently decay to an electron or muon. We included leptons from such tau decays in the fit; however, they represented less than 1% of the leptons in the one-lepton sample and form a negligible background to the two-lepton sample.

• *Errors in the lepton background estimates.* The dominant systematic error in the previous B-mixing analysis was the uncertainty in the estimation of the lepton backgrounds. Events in which one B-primary lepton combines with a misid or decay lepton to form a like-sign combination are the major source of background to the like-sign mixing signal. In this analysis, the separation of signal from background at large values of the momentum cross product and the minimum p_t variables reduces the size of this systematic effect. The signal is therefore substantially less affected by uncertainties in the exact level of

the background, and in statistical fluctuations in the background.

To check the effect on the mixing likelihood function of the misid and decay scale factors for the electron and muon samples, values which were 50% larger than those obtained from the fit were used. With these high values (leaving the other fit parameters free to vary) the value of χ obtained from the likelihood function was $\chi = 0.18^{+0.12}_{-0.08}$.

Because the majority of misid and decay leptons have small values of momentum and transverse momentum, the values of the scale factors for these components tends to be determined by the low p, p_t region of the one-lepton sample. In order to check that the estimation of the lepton backgrounds was reliable at high values of p and p_t we restricted the inclusive lepton fit to the following kinematic regions. For the one-lepton sample, leptons were required to have $p > 4$ GeV/c, $p_t > 1.5$ GeV/c, for the two-lepton sample, dileptons were required to have $mcp > 6$ (GeV/c)^2 and $min\ p_t > 1.5$ GeV/c. Although the relative amounts of C-primary, misid and decay changed (because the fit had a harder time distinguishing between them), the amount of B-primary remained unchanged. This gives us confidence that the background estimates are reliable for the region

Likelihood function for the fit to a restricted range of data

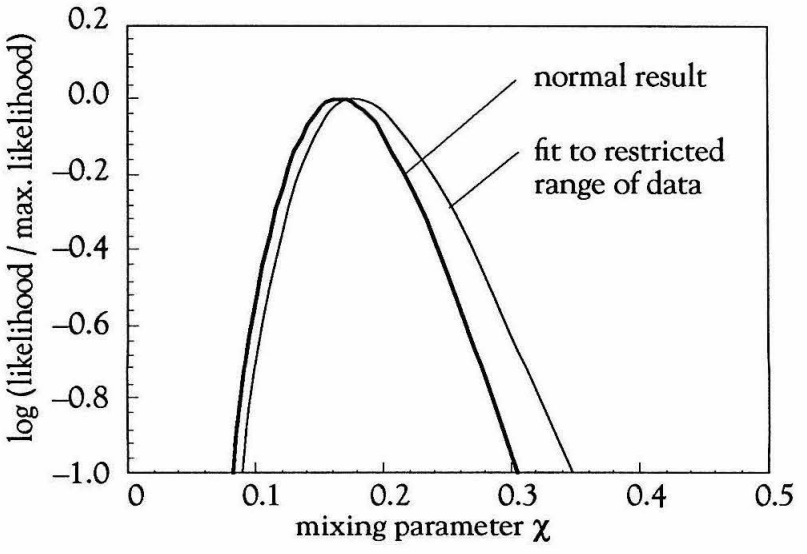

Figure 7. 1

dominated by the B-primary leptons. The likelihood function for this fit to the restricted range of data is shown in Figure 7. 1. The width of the likelihood function for the restricted fit has increased because the amount of data used has decreased, and thus the statistical precision has decreased.

Biases introduced by the procedure used to measure χ

To check that the one- and two-lepton fits were not biasing the estimation of χ, another fit was performed. This time the only contribution to the likelihood was from the observed and predicted numbers of like- and unlike-sign two-lepton events in the *mcp vs. min* p_t plane; the one-lepton data was not used in the fit. In other words, the likelihood function was maximized with respect to the eight fit variables of Table 5. 1 and the value of χ. The fit variables were free to vary within a range of $\pm$ 2 standard deviations from the values listed in Table 5. 3, where the 1 standard deviations were the statistical and systematic errors added in quadrature.

The value obtained for χ from this fit was $0.17^{+0.117}_{-0.075}$, in excellent agreement with the value obtained from the likelihood function procedure. The only fit variables which showed a significant change from their previous values were the branching ratios for $B \rightarrow e, \mu$ which had their optimal values at 12.4% and 12.7%, respectively. The correlation coefficients between χ and the each of the other parameters were all less than 0.15. Although this fit was in many ways equivalent to the "two-lepton fit" described in Chapter 5, it was a useful cross-check on the procedure and provided confidence that the estimation of χ was not strongly correlated with any of the fit variables.

• *Using a Monte Carlo sample of events with mixing.* Another important cross-check on the analysis procedure was to fit a sample of Monte Carlo events of equivalent luminosity to the hadronic data sample. The Monte Carlo was adjusted to give the correct levels of lepton background according to the estimated per track misidentification probabilities, listed in Table 3. 2 and Table 3. 5. In order to incorporate mixing into the

Monte Carlo, a random number was generated for each B-primary or B-secondary lepton. If this number was less than or equal to the required value of χ, the sign of the lepton charge was flipped. Two values for χ were used, $\chi = 0$ and $\chi = 0.25$. The likelihood functions for these samples is shown in Figure 7. 2. Both curves agree with the expected values for χ, within the statistical errors, giving us confidence that the procedure is, indeed, able to determine the value of χ.

The likelihood functions for Monte Carlo events

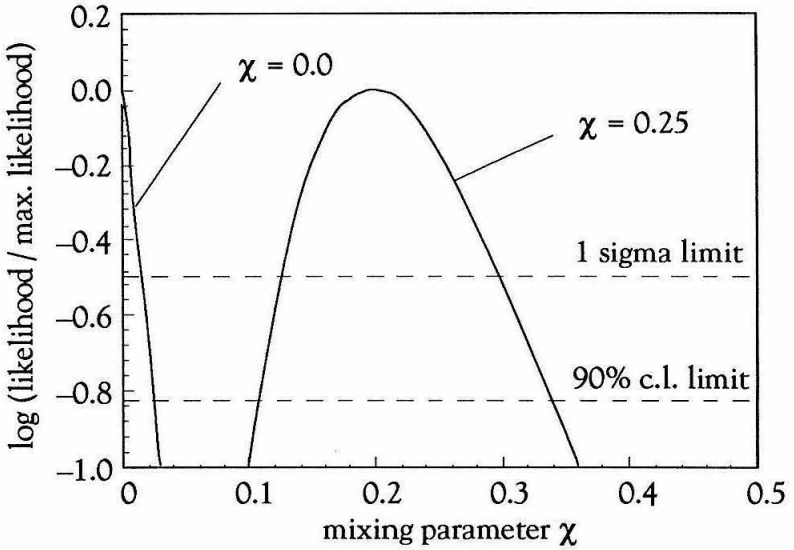

Figure 7. 2

• *The effect of the bin size.* To check that the statistical error on the number of Monte Carlo dileptons in each bin did not bias the likelihood function, a different bin size was used. Although we ensured that the number of Monte Carlo dileptons in each bin was between five and twenty-five times the number expected in the data, some statistical fluctuations might possibly have biased the result. The new bins used were the combination of four of the previous bins (2 in x, 2 in y). This reduced the total number of bins from 70 to 15. Although one would expect that increasing the bin size would reduce the sensitivity to mixing (*i.e.*, broaden the likelihood function), the most likely value should remain the same. This is shown in Figure 7. 3.

The effect of increasing the bin size in the mcp vs. min p_t plane

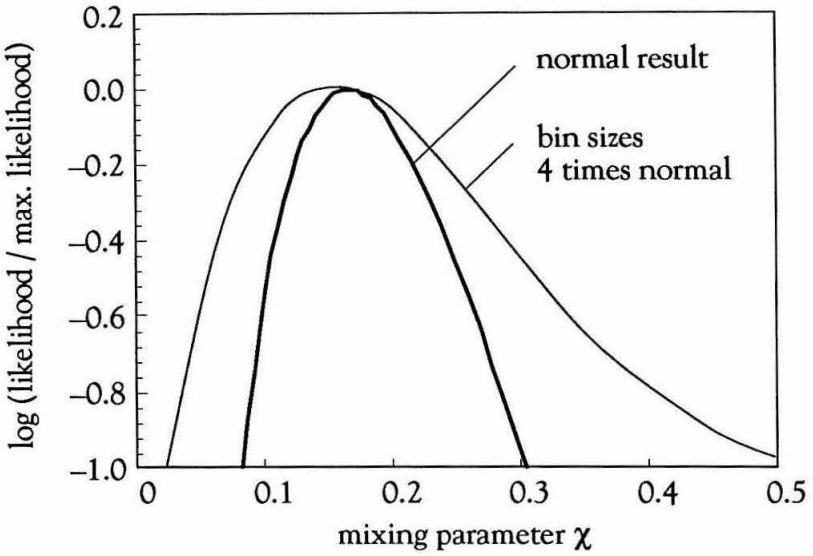

Figure 7. 3

• *The effect of separate likelihoods for ee, eμ and μμ events.* In Chapter 6 it was stated that it was important that each dilepton class have its own likelihood function, and that these three likelihood functions be added together to obtain the overall likelihood function. We show in Figure 7. 4 the effect of not considering the three classes separately, *i.e.*, summing over the lepton classes in each *mcp*, *min* p_t bin before forming the likelihood function. Since the strongest evidence for mixing is in the dimuon events, of which there were many fewer than in the other classes, a same-sign dimuon event had a much more significant effect on the mixing likelihood function than a same-sign dielectron event. Treating the three classes as equivalent thus underestimates this significance.

Assumptions about charge correlations between the dileptons.

We have listed our assumptions about the charge correlations between different dilepton types in Chapter 6. To check that our estimates for the charge correlations introduced by quark charge retention in jets did not affect the mixing result we removed this source of correlation. It made no difference to the mixing likelihood function.

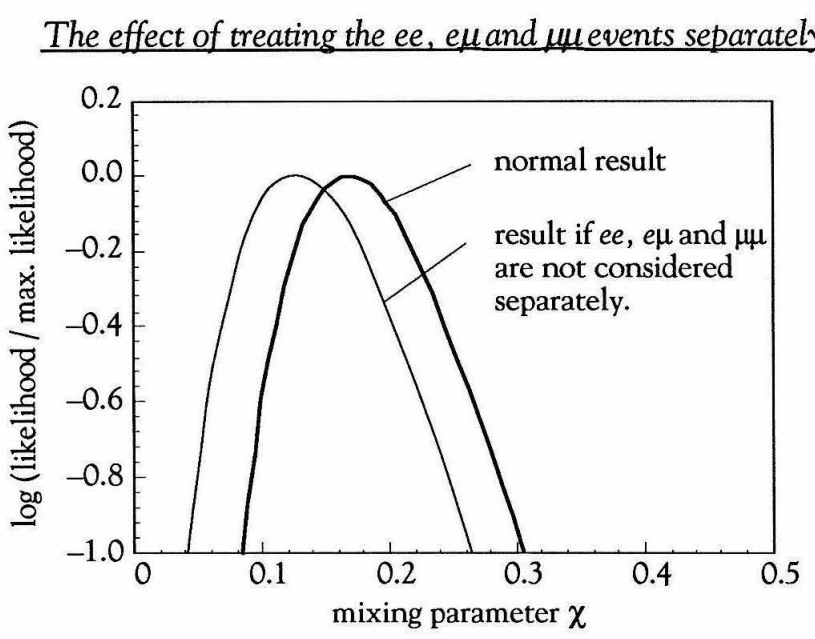

Figure 7. 4

To check the effect on the likelihood function of our assumptions about the charge correlations due to more than one charm hadron being produced in a bottom quark jet, such multiple charm production was removed. Again, the likelihood function was essentially unaffected.

Detector effects

• *Systematic tracking biases.* It is possible that the performance of the Drift Chamber and/or the tracking procedure might introduce a charge correlation between the two leptons. To investigate this, we considered two possibilities :

i) More tracks of one charge than another produced. By looking at the total numbers of positive and negative leptons in the one- and two-lepton samples, listed in Table 7. 1, it is clear that there is no significant systematic effect which leads to a greater number of tracks of one charge than another. Even if there was such a bias, it would not, to first order, lead to a charge correlation between the two leptons in the event. There does

Positive and negative leptons				
	e^+	e^-	μ^+	μ^-
$p_t < 1.0$	2437	2465	426	416
$p_t > 1.5$	496	538	304	264
$p < 2.5$	2239	2268	250	235
$p > 3.0$	867	864	511	441

Table 7. 1

appear to be a modest excess of positive muons for momenta above 3 GeV/c; however, there is no equivalent excess for the high momentum electrons. It would therefore appear that this is unlikely to be a Drift Chamber and/or tracking problem and is probably a statistical fluctuation.

ii) Mismeasurement of the charge of high momentum tracks. One can check the extent to which high momentum tracks have their charge mismeasured by looking at Bhabha events. From a detailed study of such events[32], the fraction of Bhabha tracks which have the wrong charge assignment was 0.5% for the "good" data, and 1.9% for the "poor" data†. The expected charge misassignment probability, averaged over all the data, was 0.6%. Although the tracking environment is simpler for these two-prong events, the probability that the charge of the track is mismeasured rises approximately quadratically in the track's momentum, and thus the probability for a lower momentum track to have its charge mismeasured is substantially smaller. We therefore conservatively estimate that the number of like-sign dileptons in the region of the *mcp vs. min* p_t plane sensitive to mixing (*i.e.*, *mcp* > 6 (GeV/c)^2, *min* p_t > 1 GeV/c) is less than 0.3.

• *Detector acceptance correlations.* As discussed in Chapter 5, the muon system is not azimuthally symmetric, which leads to an acceptance correlation for muon-muon events. Although this is a sizable effect, giving a 37% increase in the normalization of the dimuon spectra, the effect on the mixing likelihood function is negligible since it does not distinguish between the charges of the muons, or whether it is signal or background.

† The"poor" data consisted of ~ $25pb^{-1}$ of the total $223pb^{-1}$ of data, and was due to reduced high voltage on the Drift Chamber to alleviate dark current problems.

Chapter 8

Conclusions

In this final chapter, we compare our measurement of B-mixing with existing measurements from other experiments. Making some assumptions about the amounts of the various B hadrons present in our data sample, and using current measurements of B^0_d mixing we extract information about B^0_s mixing.

The final result

After considering all sources of systematic error, we arrived at the final result of $\chi = 0.17^{+0.15}_{-0.08}$, with 90% confidence level upper and lower limits of 0.38 and 0.06, respectively. Because of the good separation of signal and background, this result is relatively insensitive to systematic effects associated with, and statistical fluctuations in, the background.

Current experimental evidence for mixing

The existing experimental measurements and limits on B-mixing all rely on the charge of the lepton from semileptonic B decay to distinguish between b and $\overline{b}$ quark decay. The experiments can be grouped into four categories :

i) $b\overline{b}$ production in e^+e^- annihilation at $\sqrt{s}$ = 10.575 GeV on the Upsilon (4S) resonance (below the B^0_s threshold). Mixing in the B^0_d system is signaled by an excess of like-sign lepton pairs. Both ARGUS[13] and CLEO[14] have reported

measurements of substantial B^0_d–$\overline{B}^0_d$ mixing.

ii) $b\bar{b}$ production in $p\bar{p}$ annihilation at $\sqrt{s}$ = 546 and 630 GeV. UA1[33] have published a mixing measurement, where mixing was signaled by an excess of like-sign lepton pairs.

iii) $b\bar{b}$ production in e^+e^- annihilation at $\sqrt{s}$ = 29 GeV. Mixing is signaled by an excess of like-sign lepton pairs. MAC[34] has published evidence of mixing, but Mark II[35] found no evidence for mixing and published an upper limit.

iv) $b\bar{b}$ production in e^+e^- annihilation at $\sqrt{s}$ = 29 GeV. The forward-backward asymmetry in the number of muons (anti-muons) from b ($\bar{b}$) quark decays was measured. Mixing tends to dilute this effect and hence is signaled by a smaller asymmetry than expected. MAC[36] found evidence for substantial mixing, while JADE has published an upper limit.

experiment	*result*
ARGUS[13]	$\chi(B^0_d) = 0.17 \pm 0.05$
CLEO[14]	$\chi(B^0_d) = 0.16 \pm 0.04$
UA1[37]	$\chi = 0.12 \pm 0.05$
MAC[38]	$\chi = 0.21\ ^{+0.29}_{-0.15}$
MARK II[39]	$\chi < 0.12$ (90% c.l.)
MAC[36]	$\chi > 0.21$ (95% c.l.)
JADE[40]	$\chi < 0.13$ (90% c.l.)
This measurement	$\chi = 0.17\ ^{+0.15}_{-0.08}$

Table 8. 1

The current values obtained from these experiments are shown in Table 8. 1. It should be noted that the ARGUS and CLEO measurements depend on two quantities which have not been measured well, namely the ratio of B^+B^- to $B^0\overline{B}^0$ produced in Upsilon 4S decays, and the ratio of the charged to neutral B semileptonic branching ratios (it is expected that about 55% of events are B^+B^- and 45% are $B^0\overline{B}^0$, and that the charged and neutral semileptonic branching ratios are equal).

The previous Mark II mixing limit

Although this analysis shared many of the same data with the previous Mark II mixing limit[35], the approach was substantially different. The previous limit relied on using hadronic events containing one lepton to infer the number of two-lepton events, as we did. However, the previous limit used only the first 33 pb^{-1} of PEP data to obtain the background estimates. Also, our approach of using the two dimensional *mcp vs. min* p_t plane led to a much greater separation of signal from background, substantially reducing systematic errors associated with backgrounds. Finally, some sources of systematic error were previously not taken into account, namely the p_t correlations between the two leptons, and the error introduced by treating all dileptons as being equivalent (*e.g.*, a like-sign dimuon event is much more significant in terms of mixing than a like-sign dielectron event because of the different relative normalization and different backgrounds).

Production of B hadrons in e^+e^- annihilation at 29 GeV

The measurement of χ presented in this thesis is an average over all B hadrons produced in e^+e^- annihilation at 29 GeV. One of the problems of measuring B-mixing in e^+e^- annihilation above the Upsilon resonances is that it has not been possible to distinguish between the semileptonic decays of the various B hadrons produced†. There is, therefore, some uncertainty in the exact composition of the ensemble of B hadrons present in

† Mark II has been able to isolate a small sample of semileptonic B^0 decays[8] ,but this sample was far too small to be able to measure mixing.

the data. In order to extract information about the extent of B_d^0 and B_s^0 mixing, assumptions have to be made about the fractions of these mesons in the hadronic data sample.

One would expect under SU(3) flavor symmetry that equal numbers of B_d^0 and B_s^0 mesons would be produced. However, there is expected to be some suppression of strange quark production relative to up and down production due to the larger mass of the strange quark[41]. The Lund string fragmentation model, with the parameters specified in Appendix A, predicts that the composition of the sample of B hadrons which decay to B-primary leptons is 40% $B^{\pm}$: 40% B_d^0 : 12% B_s^0 and 8% B baryons. Implicit in this prediction is the assumption that these hadrons have equal semileptonic branching ratios.

Mixing is often expressed in terms of the Pais and Treiman r parameter[42], defined by :

$$r \equiv \frac{\Gamma(B^0 \to l^- X)}{\Gamma(B^0 \to l^+ X)}$$

$$\text{while } \chi(B^0) \equiv \frac{\Gamma(B^0 \to l^- X)}{\Gamma(B^0 \to l^{\pm} X)} = \frac{r}{1+r}$$

Where r_d and r_s refer to the mixing parameters for B_d^0 and B_s^0, respectively. Assuming equal semileptonic branching ratios for all B hadrons, the parameters r_d and r_s are then related to the measured value of χ and the assumed B_d^0 and B_s^0 fractions, f_d and f_s, by :

$$\begin{aligned} \chi_{measured} &= f_d \cdot \chi(B_d^0) + f_s \cdot \chi(B_s^0) \\ &= f_d \cdot \left(\frac{r_d}{1+r_d}\right) + f_s \cdot \left(\frac{r_s}{1+r_s}\right) \end{aligned}$$

To accommodate the uncertainties in the fractions of B_d^0 and B_s^0 mesons present in the hadronic data sample, we offer two possible scenarios :

	f_u	f_d	f_s	f_{other}
scenario 1	0.375	0.375	0.15	0.1
scenario 2	0.4	0.4	0.2	0.0

The quantities f_u, f_d, f_s, f_{other} are the fractions of B_u, B^0_d, B^0_s and other B hadrons (including B baryons) present in the hadronic sample.

In Figure 8. 1 we show the contours of the values of r_d and r_s for this measurement of χ, according to scenarios 1 and 2, respectively. The lightly shaded regions correspond to the part of the region allowed by the CLEO and ARGUS B^0_d measurement which is excluded at the 1 sigma level by this measurement. The dark shaded region is ruled out at the 90% confidence level. Maximal B^0_s mixing (r_s = 1) is favored, but zero B^0_s mixing (r_s = 0) cannot be ruled out at the 90% confidence level. Also shown in the figure is the 90% confidence level lower limit imposed by the UA1 measurement[33].

Summary

We have used events containing two back-to-back leptons produced in e^+e^- annihilation at 29 GeV to measure the probability that a B hadron, initially containing a *b* quark, decays semileptonically to produce a positively charged lepton. This probability, which is an average over all the produced B hadrons, was measured to be $\chi = 0.17^{+0.15}_{-0.08}$, with 90% confidence level upper and lower limits of 0.38 and 0.06, respectively. We interpret this result as evidence for the mixing of neutral B mesons. Based on the measured B^0_d mixing rate and some assumptions about the fractions of B^0_d and B^0_s mesons present in the data, this result favors maximal mixing of B^0_s mesons, although it cannot rule out zero B^0_s mixing at the 90% confidence level.

We have performed extensive checks on the lepton sample using single-lepton events to provide confidence that the sources of background are understood, and have used new variables based on the dilepton kinematics to provide good background rejection.

Limits on r_s and r_d imposed by this measurement

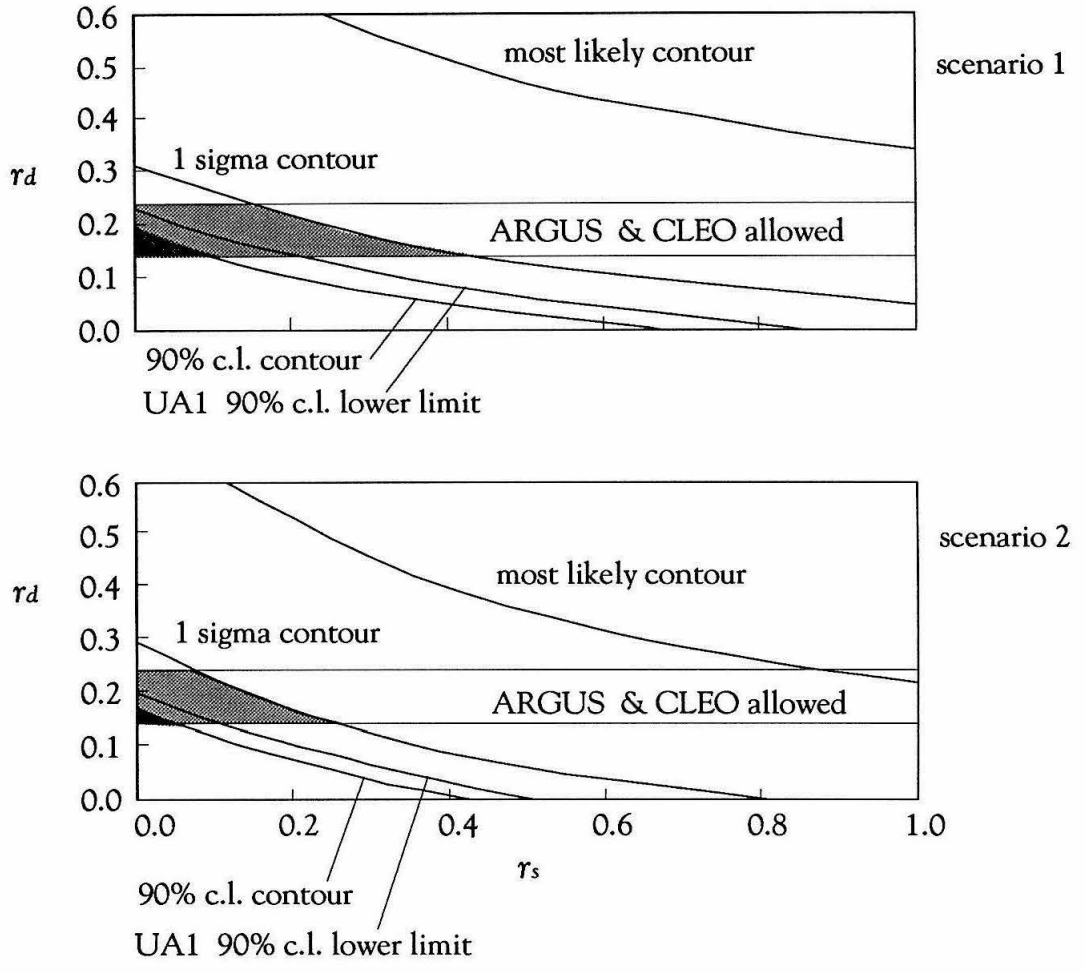

Figure 8. 1

Appendix A

The Monte Carlo

We used the Lund Monte Carlo program[30], version 6.3, to generate samples of hadronic events used in this thesis. Three distinct samples of events were generated :

- A large sample of unbiased (*udscb*) events corresponding to an integrated luminosity of ~ 255 pb^{-1}. Approximately half of these events were generated using the Lund parton shower model[43] with the Lund symmetric fragmentation function; the other half were generated using the Lund model incorporating the second order QCD matrix element[31] and the Peterson fragmentation function[2]. These two models have been shown to give good agreement with the data taken by the Mark II at 29 GeV[44].

- A large sample of $c\bar{c}$ events corresponding to approximately five times the number of $c\bar{c}$ events present in the data. These events were generated with the second order QCD matrix element model, using the Peterson fragmentation function.

- A large sample of $b\bar{b}$ events corresponding to approximately ten times the number of $b\bar{b}$ events present in the data. These events were generated with the second order QCD matrix element model with Peterson fragmentation.

The parameters used in the event generation are listed in Table A. 1. In order to increase the number of two-lepton events in the $c\bar{c}$ and $b\bar{b}$ samples, the semileptonic branching ratios for all particles containing charm or bottom quarks were increased by a factor of two.

parameter	*Lund shower Peterson fragmentation*	*2nd order m.e. Lund fragmentation*
$\Lambda_{\overline{MS}}$	0.5 GeV	0.5 GeV
y_{min}	0.015	0.015
A	0.9 (*uds* only)	0.45
B	0.7 (*uds* only)	0.9
ε_c	0.05	
ε_b	0.005	
σ_q	0.265 GeV/c	0.230 GeV/c
P_s	0.3	0.3
$P_{q\bar{q}}$	0.1	0.1

Table A. 1

Appendix

B

Calculation of the two-lepton normalization

To illustrate the calculation of the normalization factors for the two-lepton sample we choose a particular example — two-lepton events which contain a C-primary electron and a "misid" muon.

i) The Monte Carlo was used to estimate the numbers of events of each flavor present in the hadronic event sample.

ii) The total number of leptons of a given type (in this case, C-primary electrons and misid muons) in the single lepton sample was obtained from the fit parameters. The total numbers of C-primary electrons and misid muons, based on the variables in the fit, are given by :

$$\begin{aligned} \#\text{ C-primary electrons} &= Cpri_e(p, p_t) \cdot \frac{\varepsilon_{data} \cdot Br(C \to e)}{\varepsilon_{mc} \cdot Br(C \to e)_{mc}} \\ \#\text{ misid muons} &= Misid_{\mu}(p, p_t) \cdot \mu\ misid\ scale\ factor \end{aligned}$$

iii) The probability that a produced charm quark then decayed to a C-primary electron was then given by :

$$Prob(c \to \text{C-primary } e) = \frac{\#\text{ C-primary electrons}}{2 \cdot N_{c\bar{c}}}$$

and the probability that a produced charm quark decayed to a misid muon :

$$\text{Prob}\left(c \rightarrow \text{misid } \mu\right) = \frac{\#\text{ misid muons}}{2 \cdot N_{c\bar{c}}} \cdot \frac{N_{c\bar{c}}}{N_{total}}$$

where the factor of two accounts for the two quarks in each event. $N_{c\bar{c}}$ is the estimated total number of $c\bar{c}$ events, and N_{total} is the total number of events, in the hadronic event sample†.

iv) The total number of two-lepton events was then calculated from the two single-lepton probabilities. In this example, the total number of two-lepton events with a C-primary electron and a misid muon is given by :

$$N(\text{C-pri } e, \text{misid } \mu) = 2 \cdot N_{c\bar{c}} \cdot \text{Prob}\left(c \rightarrow \text{misid } \mu\right) \cdot \text{Prob}\left(c \rightarrow \text{C-pri } e\right)$$

(In this case a factor of two is necessary since the two leptons in the final state are distinguishable.)

v) This total number was then multiplied by the correction factors, described in Chapter 5.

† We have assumed here, for the sake of clarity, that the average number of misid electrons produced per event is the same for all quark flavors. In fact, because of the higher charged particle multiplicity of $c\bar{c}$ and $b\bar{b}$ events, more misid and decay leptons are produced than for $u\bar{u}$, $d\bar{d}$ or $s\bar{s}$ events. This effect was taken into consideration in the actual calculation.

[1] A clear description of the Standard Model is given in "Weak interactions of leptons and quarks" by E.D. Commins and P.H. Bucksbaum, Cambridge University Press, 1983.

[2] C. Peterson *et al.*, *Physical Review* **D27**, 105, 1983.

[3] R. Ong *et al.*, *Physical Review Letters* **60**, 2587, 1988.

[4] A review of these measurements is given in :
S. Bethke, *Zeitschrift für Physik* **C29**, 175, 1985.

[5] M. Kobayashi and T. Maskawa, *Progress of Theoretical Physics* **49**, 652, 1973.

[6] S. Glashow, J. Iliopoulos, and L. Maiani, *Physical Review* **D2**, 1285, 1970.

[7] Particle Data Group, *Physics Letters* **B204**, April 1988.

[8] Mark II have measured the lifetime of the produced ensemble of B hadrons in :
R. Ong *et al.*, *Physical Review Letters* **62**, 1236, 1989, with more details in :
R. Ong, Ph.D thesis, SLAC-Report-320, 1987.
They have also measured the lifetime of a sample of neutral B mesons in :
S. Wagner *et al.*, to be submitted to *Physical Review Letters*.

[9] For a clear discussion of K^0– $\overline{K}^0$ mixing see chapter 7 of ref. [1].

[10] A theoretical discussion of CP violation in the K^0–$\overline{K}^0$ and B^0–$\overline{B}^0$ systems is given in : M. Wise, CALT-68-1514, 1988.

[11] L. Wolfenstein, *Communications in Nuclear and Particle Physics* **14**, 135, 1985.

[12] M.K. Gaillard and B.W. Lee, *Physical Review* **D10**, 897, 1974.
M.K. Gaillard *et al.*, *Reviews of Modern Physics* **47**, 277, 1975.

[13] H. Albrecht *et al.*,(ARGUS Collaboration), *Physics Letters* **B192**, 245, 1987.

[14] A. Jawahery (CLEO Collaboration), Proceedings of the XXIV International Conference on High Energy Physics, Munich, 1988.

[15] The uncertainty in the predicted top quark mass is more than a factor of four. See, for example : I. Bigi, SLAC-PUB-4521, 1988.

[16] R. Ong, Ph.D. thesis, Stanford University, SLAC-Report-320, 1987.

[17] The cluster finding algorithm is described in detail in :
S. Bethke *et al.*, *Zeitschrift für Physik* **C43**, 331, 1989.

[18] The pre-upgrade (PEP 5) detector is described in :
R. Schindler *et al.*, *Physical Review* **D24**, 78, 1981, and
B. LeClaire, Ph.D. thesis, Stanford University, SLAC-Report 321, 1987.
The Upgraded detector is described in :
G. Abrams *et al.*, *Nuclear Instruments and Methods* **A281**, 55, 1989.

[19] More details about the Drift Chambers can be found in :
W. Davies-White *et al.*, *Nuclear Instruments and Methods* **160**, 227, 1979,
J. Jaros, in *Proceedings of the International conference on Instrumentation for Colliding Beam Physics*, edited by W. Ash (Stanford Linear Accelerator Center, Stanford, CA), 1982 , and
R.Ong, Ph.D. thesis , Stanford University, SLAC-Report 320, 1987.

[20] More details about the Liquid Argon calorimeter can be found in :
D. Karlen, Ph.D. thesis, Stanford University, SLAC-Report 325, 1988.

[21] W.T. Ford *et al.*, *Nuclear Instruments and Methods* **A255**, 486, 1987.

[22] The electron and muon identification algorithms are described in detail in :
M. Nelson, Ph.D. thesis, University of California, Berkeley, LBL-16724, 1983.

[23] Details of the electron identification efficiency measurement, and the selection of tau pair events, can be found in :
P. Burchat, Ph.D. thesis, Stanford University, SLAC-Report-292, 1986.

[24] We used the hadronic interaction simulation program FLUKA, described in :
P.A. Aarnio, A. Fasso, H-J. Möhring, J. Ranft, and G.R. Stephenson, CERN-TIS-RP/168, 1986 (unpublished).
This implementation of the Monte Carlo is described in detail in :
A.J. Weir, Mark II/SLC note # 193, December 1987 (unpublished).

[25] P.C. Rowson, Ph.D. thesis, University of California, Berkeley, LBL-20463, 1985.

[26] F.A. Berends, P.H. Daverveldt and R. Kleiss, *Nuclear Physics* **B253**, 441, 1985;
P.H. Daverveldt, Ph.D. Thesis, University of Leiden, 1985;
F.A. Berends, P.H. Daverveldt and R. Kleiss, *Computer Physics Communications* **40**, 271, 1986.
These Monte Carlo tapes were originally made by René Ong and Tim Barklow.

[27] The tau-pair tapes were made by Sterling Watson.

[28] The World Average values for the semileptonic branching ratios were obtained from René Ong's thesis, SLAC-Report-320, 1987.

[29] Quark charge retention in jets has been measured by :
T. Schaad, Ph.D. thesis, Harvard University, October, 1985.

[30] T. Sjöstrand, *Computer Physics Communications* **39**, 347, 1986;
T. Sjöstrand and M. Bengtsson, *Computer Physics Communications* **43**, 367, 1987;
M. Bengtsson and T. Sjöstrand, *Nuclear Physics* **B289**, 810, 1987.

[31] T.D Gottschalk and M.P. Schatz, *Physics Letters* **B150**, 451, 1985.
T.D Gottschalk and M.P. Schatz, CALT-68-1172,-1173, -1199, 1985.

[32] D. Karlen, Ph.D. thesis, Stanford University, SLAC-Report-325, 1988.

[33] C. Albajar *et al.* (UA1 Collaboration), *Physics Letters* **B186**, 247, 1987.

[34] H. Band *et al.*(MAC Collaboration), *Physics Letters* **B200**, 221, 1988.
R. Hurst, Ph.D. thesis, RX-1203, University of Houston, 1987.

[35] T. Schaad *et al.*(Mark II Collaboration), *Physics Letters* **D160**, 188, 1985.
T. Schaad, Ph.D thesis, Harvard University, October, 1985.

[36] R. Hurst *et al.*, *Physics Letters* **B218**, 369, 1989.

[37] C. Albajar *et al.* (UA1 Collaboration), *Physics Letters* **B186**, 247, 1987.

[38] H. Band *et al.*(MAC Collaboration), *Physics Letters* **B200**, 221, 1988.
R. Hurst, Ph.D thesis, RX-1203, University of Houston, 1987.

[39] T. Schaad *et al.*(Mark II Collaboration), *Physics Letters* **D160**, 188, 1985.
T. Schaad, Ph.D thesis, Harvard University, October, 1985.

[40] W. Bartel *et al.* (JADE collaboration), *Physics Letters* **B146**, 437, 1984.

[41] W. Bartel *et al.*, *Zeitschrift für Physik* **C20**,317, 1983.
H. Aihara *et al.*, *Physical Review Letters* **44**, 10, 1984.

[42] A. Pais and S.B. Treiman, *Physical Review* **D12**, 2744, 1975.

[43] B. Anderson *et al.*, *Physical Review* **97**, 33, 1983.

[44] A. Peterson *et al.*, *Physical Review* **D37**, 1, 1988.